2016

Modulation of Watershed Nutrient Loads By Tidal Creek Ecosystems on The Virginia Eastern Shore

Britt Leighanne Dean
College of William and Mary - Virginia Institute of Marine Science, brittley@gmail.com

Modulation of Watershed Nutrient Loads by Tidal Creek Ecosystems on the
Virginia Eastern Shore

––––––––––

A Thesis

Presented to

The Faculty of the School of Marine Science

The College of William and Mary in Virginia

In Partial Fulfillment

of the Requirements for the Degree of

Master of Science

––––––––––

by

Britt Leighanne Dean

August 2016

APPROVAL PAGE

This thesis is submitted in partial fulfillment of

the requirements for the degree of

Master of Science

Britt Leighanne Dean

Approved by the Committee, July 2016

Mark J. Brush, Ph.D.
Committee Chair / Advisor

Iris C. Anderson, Ph.D.

Jian Shen, Ph.D.

Walter R. Boynton
University of Maryland Center for Environmental Science
Solomons, Maryland

This M.S. is dedicated to my family, especially Mom, Alan, and Kelsey. Thank you for always supporting me in every endeavor I undertake.

TABLE OF CONTENTS

ACKNOWLEDGEMENTS

I would like to thank my advisor and fearless leader, Dr. Mark Brush, for all of the big science! I have learned so much from working with Dr. Brush and I am a better scientist for it. I would also like to thank Dr. Sam Lake, the Coastal Systems Ecology and Modeling Lab Guru. The open door policy and dedication to teaching exhibited by Dr.'s Brush and Lake contributed to my successful completion of my M.S. thesis project.

Additionally, I could not have accomplished this thesis project without the ever present help of the folks in Dr. Iris Anderson's Lab group. Hunter Walker worked tirelessly for a year to conduct monthly dataflow cruises and run all of the nutrient samples. Jen Stanhope was instrumental in development of the field monitoring program as well as data processing and QAQC. Jen also provided me with unlimited advice during the project and was always available to answer my questions.

My committee members, Jian, Iris, and Walter, were also extremely helpful and patient through the process of completing my degree. They made for an incredibly knowledgeable group of mentors.

Last but certainly not least I would like to thank all of the members of the Coastal Systems Ecology and Modeling Lab for unlimited help with sample processing, brainstorming, and general support. Thank you Brittani Koroknay, Sara Blachman, Michael Kushner, Shanna Williamson, Emily Egginton, Alma Ramirez, and Jennifer Radcliffe.

LIST OF FIGURES

LIST OF TABLES

ABSTRACT PAGE

While deeper estuaries typically demonstrate predictable responses to increased nutrient loads, responses in shallow systems are more varied, due in part to the presence of multiple benthic autotrophs. Shallow systems are particularly vulnerable to increases in watershed nutrient loads due to their position at the interface between land and open water. The prevailing conceptual model of eutrophication for shallow systems currently describes a succession in the dominant autotroph from seagrass to macroalgae to phytoplankton, but this model does not include benthic microalgae, which can sequester nutrients in photic systems. The Virginia Eastern Shore is characterized by shallow lagoons connected to upland watersheds through small tidal creeks, where the main source of fresh water and nutrients is groundwater. While some studies have characterized the response of the lagoons to nutrient loads, little is known about the tidal creeks and whether they act as filters, transformers, or conduits for land-based nutrients. We examined the role tidal creeks play in modulating watershed nutrient inputs in the Great Machipongo River (GMR) system, the largest tidal creek complex on the seaside of the Virginia Eastern Shore. We developed a field monitoring program that provided data to calibrate a reduced complexity Estuarine Ecosystem Model (EEM). Production, respiration, and net ecosystem metabolism were quantified, using both the open water and component methods, seasonally at three sites within this system. These rates together with monthly concentrations of standing stock nutrients and water column chlorophyll, monthly DataFlow surveys of physiochemical parameters, seasonally and spatially-intensive benthic chlorophyll surveys, and a bathymetric survey were used to develop and calibrate the EEM. The model was used to assess the degree to which tidal creeks export (via flushing), remove (via denitrification), or transform (via autotrophic uptake) land-based nutrient loads to the adjacent lagoons during baseflow and storm conditions. Component metabolism studies showed the system was overall net autotrophic, with increasing dominance of benthic processes towards the head of the estuary. Open water metabolism studies suggested the system was overall net heterotrophic, but we believe this conclusion is biased by the surrounding marshes and violations of the constant water mass assumption. The creek system exported 61,476 kg N y-1 as phytoplankton biomass, an amount approximately equal to inputs from the watershed and atmosphere, and imported 172,830 kg N y-1 in dissolved inorganic forms for a net import of 111,354 kg N y-1 from Hog Island Bay. Phytoplankton uptake, benthic microalgal uptake, and denitrification accounted for 216%, 343%, and 38% of the annual input of watershed and atmospheric N to the system, indicative of rapid cycling and advection of nutrients from Hog Island Bay. The storm simulation showed that almost all of the additional 28,635 kg N y-1 added from the watershed was flushed to Hog Island Bay and a small portion was denitrified. This study indicates that GMR system function is dominated by benthic processes, and the system acts as a transformer and filter of land-based nutrients during normal conditions and a conduit of nutrients during storm conditions.

Modulation of Watershed Nutrient Loads by Tidal Creek Ecosystems on the
Virginia Eastern Shore

INTRODUCTION

I.   *Eutrophication in Coastal Systems*

Human influence on the coastal zone has become a worldwide issue. Inherent in the functioning of temperate marine systems is a limitation of autotrophic growth by nitrogen availability, and land use change with an associated increase in nutrient loading can have a major impact on coastal ecosystem function (Howarth 1988, Nixon 1995, Rabalais et al. 2002, Howarth and Marino 2006). This increase in nitrogen load typically results in eutrophication, defined as "an increase in the rate of supply of organic matter to an ecosystem", which in turn causes varied responses in coastal systems (Nixon 1995). The classic response in relatively deep, plankton-based estuaries is enhanced productivity and biomass of phytoplankton (Nixon et al. 2001). In addition to direct effects of nutrient loading, indirect effects include a decrease in light availability needed for autotrophic growth and bottom water hypoxia due to decomposition of excess biomass (Cloern 2001). Other typical symptoms of late stage eutrophication include altered metabolic functioning, harmful algal blooms, fish kills, and loss of benthic vascular plants and associated species (Cloern 2001, Testa et al. 2008; Kemp and Testa 2011).

While deeper estuaries tend to exhibit predictable responses to nutrient inputs, these relationships have proven more elusive in shallow lagoonal systems (Nixon et al. 2001). Much of the global coastline including the U.S. Atlantic and Gulf coasts is

fringed by these shallow lagoonal systems which exhibit variable responses to eutrophication. Our changing conceptual model of eutrophication now includes system attributes such as tidal energy, residence time, light availability, and presence of filter feeders, that can mediate the response to nutrient loading, acting as 'filters' between increased loading and system response (Cloern 2001). One main characteristic that distinguishes shallow systems from deeper systems is a photic zone that extends to the sediments, thus stimulating benthic primary production and enhancing benthic-pelagic coupling of biogeochemical cycles (McGlathery et al. 2007).

Tidally influenced creeks are often positioned at the interface between the land and adjacent lagoons, making them particularly susceptible to nutrient inputs from changing land use (Anderson et al. 2010). These zones of transition are also important sites of nutrient processing with sometimes extremely high turnover rates of nitrogen (Buzzelli 2008). High rates of denitrification in these shallow systems can also act as a major nitrogen sink, with average rates between 1 and 10 mmol $m^{-2} d^{-1}$ and reported rates up to 30 mmol $m^{-2} d^{-1}$ (Joye and Anderson 2008). These systems have the potential to act as conduits, transformers, or filters for land-based nutrient inputs as they transit to the adjacent lagoons. Given their small volumes and relatively rapid flushing rates, these creeks may act as conduits that rapidly flush land-based nutrients into the adjacent lagoons where they may have negative impacts. Alternatively, tidal creeks may exhibit typical responses associated with eutrophication such as phytoplankton blooms which transform land-derived nutrients into particulate and organic forms that are subsequently flushed to the lagoons. Finally, these creeks could act as efficient filters or traps for land-based loads through denitrification and immobilization by benthic microalgae. Due

to their proximity to land, the first warning signs of human impact on estuarine systems could appear in these creeks, making study of their function of major importance.

II.   *Characteristics of Shallow Systems*

One reason shallow systems respond to nutrient enrichment differently than deeper systems is the relative time it takes water to enter and subsequently leave the system. Flushing or residence time can control system dynamics and thus the fate of nutrients entering the system. In a compilation of multiple systems, Nixon et al. (1996) found that with increased residence times the percent of total nitrogen inputs that were subsequently exported from the system decreased. Flushing time is an "integrative system parameter that describes the general exchange characteristics of a waterbody", and is often the most useful and easily calculated metric of transit time in an estuarine system (Monsen et al. 2002). Typical flushing or residence times for deep systems like Narragansett and Chesapeake Bays are on the order of weeks to several months, whereas values for shallow systems are often on the order of days to weeks, with notable exceptions such as Chincoteague Bay, MD/VA: a shallow system with a residence time of 2-3 months (Pritchard 1960; Nixon et al. 2001; Herman et al. 2007; Wang 2009).

There are two widely used methods for calculating flushing time of an estuary: the freshwater fraction method, which utilizes river flow, volume of the system, and a salt balance (Shen and Wang 2007), and where river inflow is not well known or tidal range is large, the tidal prism method (Monsen et al. 2002). Both calculations assume a well-mixed system, and the tidal prism method has a singular assumption that the tidal volume

of water is replaced on every subsequent tide with new water (Fugate et al. 2005). This

assumption can be addressed by introducing a coefficient β which represents the percent

of exiting water that returns on the next flood tide, but this coefficient is difficult to

estimate thus the tidal prism method may underestimate flushing time (Monsen et al.

2002; Fugate et al. 2005; Herman et al. 2007).

Flushing time also affects phytoplankton primary productivity, which is

contingent on the balance between growth and loss, although Lucas et al. (2009) point out

that transport time is not always the main control of phytoplankton growth and loss.

Systems can switch between growth and loss dominance seasonally or annually, and the

balance can be controlled by a combination of flushing time, presence of grazers, and

nutrient delivery (Lucas et al. 2009). In San Francisco Bay, Alpine and Cloern (1992)

found changes in primary production and biomass varied not only with physical

dynamics but also with the presence or absence of bivalves in the system, on a seasonal

and yearly time scale.

Shallow systems also differ from deep systems due to the varied roles played by

multiple autotrophs. A compilation of estuarine primary production rates showed that

most estuaries fall between 100-300 g C $m^{-2} y^{-1}$ (Boynton and Kemp 2005). Because

most of these rates are pelagic, the authors include data sets from Borum and Sand-

Jensen (1996) that represent total system primary productivity from very shallow systems

that include benthic rates.   In this analysis, most systems fell between 300 and 400 g C

$m^{-2} y^{-1}$, emphasizing the important role of benthic autotrophs in addition to water column

autotrophs. In a similar comparison of metabolic rates for shallow lagoons, McGlathery

et al. (2001) found that systems including benthic autotrophs had much higher rates of primary production than those only containing water column atutotrophs.

Given their position on the bottom, benthic autotrophs have ready access to water column nutrients as well as nutrients in the sediments (Boynton and Kemp 2005). Because of this, benthic microalgae (BMA) can play a large role in nutrient cycling in shallow systems. Anderson et al. (2003) found that BMA can act as a sink for water column nitrogen when the metabolic nitrogen demand of the BMA exceeds that supplied by mineralization in the sediments. This study also showed that macroalgal nitrogen uptake can be important at certain times of the year (Anderson et al. 2003). Although this nitrogen removal can be a large sink, these macroalgal blooms can also cause a shift in the dominant autotroph due to shading of the benthos, which affects biogeochemical cycling due to the different fates of various benthic autotrophs (McGlathery et al. 2007). Biomarker studies conducted by Hardison et al. (2011) showed that although macroalgae act as a sink for carbon and nitrogen, this is only a temporary phenomenon and after the late-summer die off of macroalgae the carbon and nitrogen is cycled back into the system. Some of this carbon and nitrogen can then be sequestered by the sediments, but the amount is heavily dependent upon tides and waves working to suspend macroalgae into the water column or export it from the system (Hardison et al. 2010).

III.   *Coastal Systems of the Delmarva Peninsula*

The coastal bays and associated tributaries on the Eastern Shore of Virginia are typical back-barrier lagoons with shallow depths, small watersheds, and limited

connections to the adjacent ocean through narrow inlets. While many tidal creek systems

face intensified urban or residential development, the creeks on the Eastern Shore mainly

face intensified agriculture. The main type of agriculture in this area has shifted in the last

10-15 years from traditional row crops including corn, soy, and sweet potatoes, to more

intensive tomato plasticulture and chicken husbandry. Accomack County issued permits

for 43 new poultry houses between 2001 and 2007, a significant addition for the size of

the county which pushed its rank to third largest broiler chicken producing jurisdiction in

the Commonwealth of Virginia (Accomack County 2010). Tomatoes produced on the

Virginia Eastern Shore are now estimated to constitute 80% of the total grown in the

Commonwealth of Virginia (Northampton County 2009). This change in agricultural use

has the potential to leach excess nitrogen into the receiving waterways and groundwater

given the more intensive nature of these activities relative to row crop agriculture

(Giordano et al. 2011).

Land use in the Virginia portion of the Delmarva Peninsula is less impacted than

the more urban and heavily agricultural landscape to the north, comprised mostly of

unchanged natural habitat (including wetlands), followed by agricultural uses and very

little urban cover (Stanhope et al. 2009; Anderson et al. 2010). Although both Accomack

and Northampton counties have previously experienced population growth, the results of

the 2010 U.S. Census confirmed a decreased population in both counties (Northampton

County Comprehensive Plan Advisory Committee 2013, Accomack County 2014). Both

counties now predict stagnant growth or a slight decrease in population with a subsequent

stagnation of development for the foreseeable future (Accomack County 2008 and 2014;

Northampton County 2009; Northampton County Comprehensive Plan Advisory Committee 2013).

The seaside region of the Virginia Eastern Shore is characterized by unconsolidated sandy soils and shallow aquifers (Robinson and Reay 2002). Due to the morphology of the coastal lagoons and the small area of the peninsula, the Virginia Eastern Shore is characterized by lagoons with small ratios of watershed to lagoon area (Anderson et al. 2010; Giordano et al. 2011). Since the main source of freshwater to these systems is groundwater, the connection between land use and ecosystem function is especially enhanced, although difficult to assess (Robinson and Reay 2002, Stanhope et al. 2009, Anderson et al. 2010). Residence time is estimated to be on the order of days to weeks for Hog Island Bay and the majority of the seaside lagoons on the Delmarva Peninsula (Fugate et al. 2005; Herman et al. 2007). Lying between the uplands and outer lagoons are small tidal creeks, ubiquitous along the entire Delmarva. These creeks flow from agricultural fields and forested uplands at their heads to broad salt marshes along the mainstem and mouths of the creeks. All systems on the Delmarva are well mixed and heavily influenced by tides, due to the approximately 1.2 meter tide range and small amount of freshwater input (tidesandcurrents.noaa.gov). In addition to uptake by BMA, macroalgae, and denitrification discussed above, the Eastern Shore is characterized by extensive intertidal marshes, which can be a proportionally large sink for nitrogen per unit area. Boynton et al. (2008) found that although marshes comprised only 27% of system area in the Patuxent River, MD, they removed a proportionally larger 46% of the external nitrogen load (Boynton et al. 2008).

Along with chicken husbandry and tomato plasticulture, another rapidly growing sector within the agricultural industry in Accomack and Northampton counties is shellfish aquaculture (Accomack County 2008; Northampton County 2009). The seafood industry has long been an important part of the economy of the Virginian Eastern Shore, but has been decreasing in importance with declining fish stocks in recent decades. Shellfish aquaculture is a rapidly increasing industry in these counties, and is cited as the main potential business growth sector (Accomack County 2008; Northampton County 2009). Shellfish aquaculture requires healthy waterways and has been at odds with other components of the agriculture industry on the Eastern Shore, with shellfishermen citing runoff from tomato plasticulture farms as being harmful to their operations (Accomack County 2008; Northampton County 2009). This is an area of concern for local managers on the Eastern Shore and both counties plan to simultaneously promote growth of the tomato plasticulture and chicken husbandry industries while maintaining high water quality in the creeks and bays utilized for aquaculture (Accomack County 2008; Northampton County 2009).

While anthropogenic impacts on the Delmarva Peninsula tend to increase from south to North, a recent application of a Nitrogen Loading Model (NLM) along the Peninsula found that some Virginia bays are indeed moderately impacted due to intensive agriculture and localized point sources (Brush 2010; Giordano et al. 2011). Nitrogen loading has been shown to increase chlorophyll *a* and total nitrogen concentrations in the coastal bays of Maryland (Boynton et al. 1996). Utilizing the relationships found in the Maryland bays and nutrient loading predicted by the NLM, Giordano et al. (2011) calculated expected chlorophyll-a and total nitrogen (TN) concentrations for the Virginia

bays. These predicted concentrations disagreed with monitoring data in these systems, suggesting that the Virginia bays do not respond to increased nitrogen loads in the same manner as the more impacted Maryland bays. However, another explanation for this discrepancy is that Giordano et al.'s (2011) sampling in the Virginia bays was focused on open waters of the lagoons and did not extend into the tidal creeks, while the Boynton et al. (1996) study utilized data from more nearshore and upstream locations. It is also possible that the tidal creeks in Virginia exhibit symptoms of eutrophication before the nutrients reach the lagoons, or are acting as strong nutrient sinks preventing their transit to the lagoons.

IV.   *Tools for Understanding Shallow Systems*

a. Ecosystem Metabolism

In defining how coastal systems function, an assessment of whole system metabolism can answer some basic questions about the system while also helping to steer research objectives. Net Ecosystem Metabolism (NEM) is a measure of the trophic status of a system, defined as the balance between the rate of Gross Primary Production (GPP) and Respiration (R), and quantifies the energy available for transfer to higher trophic levels (Kemp and Boynton 1980; Staehr et al. 2012). NEM is a useful metric for determining if a system is supported by inorganic nutrients or organic terrestrial materials and assessing the fate of allochthonous and autochthonous inputs to the system (Kemp and Testa 2011; Staehr et al. 2012). Net autotrophic systems have higher rates of production than

respiration and require inputs of inorganic nutrients, while net heterotrophic systems

exhibit higher rates of respiration than production, requiring a source of organic matter to

the system (Caffrey 2003; Kemp and Testa 2011). Autotrophic systems export organic

matter and act as a source for fixed carbon, while heterotrophic systems export nutrients

and act as a sink for fixed carbon (Kemp and Testa 2011).

Comparisons of NEM can be made among multiple systems or over time within the

same system, but because of high levels of variance and diverse ecological drivers in

coastal systems, this is not always possible. In an attempt to characterize the metabolic

state of any system and to understand how NEM responds to different environmental

factors, multiple assessments must be made to identify and understand the relationship

between biological processes and the driving physical and environmental factors.

Two main methods used to characterize the NEM of a system include the open water

and component methods. Both methods can use CO_2/pCO_2 or dissolved oxygen (DO) as

tracers of biological activity, as they are involved in both respiration and photosynthesis

(Caffrey 2003). While changes in DO concentrations may not fully reflect total

respiration in the system if there are high rates of anaerobic respiration occurring in the

sediments, DO-based rates partially account for anaerobic respiration because the

reduced byproducts tend to get oxidized as they diffuse upward through the sediments

(Hopkinson and Smith 2005, Testa et al. 2013).

Open Water Method: A widely used method of calculating NEM involves integrating

the entire system using continuously monitoring DO sensors. This open water method

relies on the assumption that the water moving past the DO sensor is representative of the

same water mass throughout the deployment, but this is often difficult to discern in

estuaries. The DO sensors are often deployed for extended periods of time and at multiple sites to achieve adequate temporal and spatial resolution (Caffrey 2003, Kemp and Testa 2011). Many studies incorporate DO profiles, or DO data from multiple depths, in order to determine the similarity of water masses along horizontal and vertical gradients (Kemp and Testa 2011; Staehr et al. 2012).

Dissolved oxygen percent saturation and concentration from successive time steps are used to calculate rates of production or consumption following correction for air-sea diffusion (Kemp and Testa 2011). Net community production (NCP) is defined by changes in DO during daylight hours or hours of positive production rates. Community respiration rates are defined by changes in DO during night time hours. Gross Primary Production (GPP) is defined as NCP plus R. These rates can be computed each measurement interval (e.g., every 15 minutes) or using averages over longer intervals (e.g., hourly) to smooth out any anomalies, and are then summed to obtain daily rates.

Component Method: The component method of assessing NEM involves isolating parts of the system, analyzing each separately, and combining their rates to obtain NEM. Production and respiration rates are measured for the sediments, water column, and depending on the system, seagrasses, marshes, and/or macroalgae. Although these can be measured in situ or in the lab, these experiments are more commonly conducted in the lab due to logistical constraints (Hopkinson and Smith 2005).

Water, sediment, and plant samples are collected in bottles and incubated in light and dark conditions for NCP and R, respectively. As with the open water measurements, changes in DO concentrations over time are converted to rates, with light and dark readings providing estimates of NCP and R, respectively (Hopkinson and Smith 2005).

These rates are then scaled up to the whole system and combined to obtain total system rates of GPP and NEM. In order to address the bottle effects associated with lab experiments, bottle incubations are kept short to avoid the buildup of metabolites and the deficit of reactants.

b. Ecosystem Simulation Models

Studies that incorporate synthesis of data and/or models can answer ecological questions by identifying drivers among systems, within a single system, and along a temporal gradient. A recent paper by Kemp and Boynton (2012) highlighted the importance of this type of research in coastal systems, and defined synthesis as, *"the inferential process whereby new models are developed from analysis of multiple data sets to explain observed patterns across a range of time and space scales."* Mathematical simulation models provide one key tool for conducting synthesis research by combining known properties of a system with ecological principles to answer pressing ecological questions (Kemp and Boynton 2012, Brush and Harris 2016). These models range in complexity from simple linear regressions describing the relationship between two parameters up to highly complex and spatially resolved models such as those used by the Chesapeake Bay Program (Cerco and Cole 1994; Brush and Harris 2016).

Process-based models incorporate formulations of rate processes based on ecological principles rooted in theory or direct measurements. These models represent a mechanistic understanding of the system and can be used to determine biological, physical, and chemical controls on system dynamics. As discussed in Nixon et al.

(2009), one such model was used in Narragansett Bay to identify a possible cause of a

fundamental shift in benthic-pelagic coupling within the system (Kremer and Nixon

1978). By varying one parameter of the model while keeping the others constant, the

authors found that light and not temperature was driving a shift in the timing of the

winter-spring phytoplankton bloom, contributing to an uncoupling of the benthos and

water column (Nixon et al. 2009). A similar model applied in the York River Estuary,

VA found that hypoxia in the lower estuary was partially driven by advection of

dissolved organic carbon from the Chesapeake Bay, which has major implications for

management of hypoxic events (Lake and Brush 2015).

These mechanistic understandings of system function are critical in creating

management strategies and understanding the consequences of human actions in coastal

zones. In addition to explaining how a system is currently functioning, models have the

ability to predict how future changes will impact the system and associated resources,

while identifying areas in need of further study.

OBJECTIVES

Given our lack of understanding of the role of tidal creeks in modulation of land-based nutrient loads, the purpose of this project was to combine field measurements of water quality and ecosystem metabolism with model simulations to quantify the degree to which a representative creek system acts as a nutrient conduit, transformer, or filter. Through model simulations and mass balance computations this project quantified the response of the study system to current land-based nutrient loads and identified its role in modifying watershed loads before they reach the adjacent lagoon. Specific objectives and hypotheses were:

Objective 1: Assess NEM at multiple sites within a representative tidal creek system to quantify trophic status.

> *Hypothesis 1:* Given the high levels of light, intermediate concentrations of nutrients, and fast flushing rates of the seaside Virginia tidal creeks, NEM will trend towards net autotrophy.

Objective 2: Simulate creek function using an ecosystem model to assess the role of tidal creeks in removing, transforming, and exporting nutrient inputs from the upland watershed.

Hypothesis 2a: Benthic processes in the system will serve to modulate nutrient loads from groundwater seepage.

Hypothesis 2b: Water column production will be low during baseline conditions and times of low surface runoff when BMA retention of nutrient loads from groundwater will dominate primary production in the system.

Hypothesis 2c: During times of high freshwater input, the high levels of tidal exchange will serve to export water column nutrients to the adjacent lagoon systems.

MATERIALS AND METHODS

Site Selection

The Great Machipongo River (GMR) system and its tributaries on the seaside portion of the Virginia Eastern Shore form the largest tidal creek system in the region (Fig 1). Multiple tributaries flow into the Machipongo River including Greens, Upshur, and Partings Creeks, and the system drains into Hog Island Bay. These tributaries are characterized by little fresh water input, short residence times (days to weeks), extensive marshes and mudflats, and differing land use within each aquifer recharge zone (Herman et al. 2007; Stanhope et al. 2009; Anderson et al. 2010). Groundwater inputs to the GMR are the main source of fresh water to Hog Island Bay which receives a low rate of nitrogen loading (4.5 kg N ha^{-1} y^{-1}; Anderson et al. 2010) primarily from non-point sources. The watershed of Hog Island Bay is mostly natural vegetation (60%) and agriculture (31%) with very little impervious surface (7%) (Giordano et al. 2012).

The GMR was the site of monthly water quality surveys during 2012-13 led by Dr. Iris Anderson's lab at VIMS as part of Virginia Sea Grant project R/715165, providing an annual cycle of measurements for development and calibration of an Estuarine Ecosystem Model (EEM, see below). As the largest creek system on the seaside of the Virginia Eastern Shore, the Machipongo River also provided the greatest chance of observing salinity gradients which facilitates application of the EEM.

Additionally a version of the EEM is already running in the adjacent lagoon (Hog Island Bay; Brush 2014). The system is quickly flushed due to its shallow nature combined with a 1.23 m mean daily tide range at nearby Wachapreague, VA (NOAA tide station 8631044).

Tidal Creek Characterization

I.   *Creek Box and Watershed Delineation*

Using aerial images, knowledge of the system vegetation, and high resolution shapefiles from the USGS National Hydrography Dataset (NHD), a new digitization of the Machipongo creek complex was created in ArcGIS 10.1 and included divisions for marsh, subtidal shoal, and channel areas. For purposes of the model, the system was divided into five coarse scale creek boxes, using natural constrictions and changes in bathymetric profiles as guidelines: Partings Head (PH), Machipongo Head (MH), Machipongo South of Bridge (MSB), Machipongo Intermediate (MI), and Machipongo Mouth (MM) (Fig 1; Table 1). Once creek boxes were defined, the watershed for each box was then delineated using an existing watershed file for Hog Island Bay (Brush et al. 2015), aerial images, and NHD flowline data (Table 1).

II.   *Bathymetric Mapping*

On June 15, 2015, a depth survey was conducted using a skiff outfitted with a sonar capable GPS unit (Garmin GPSmap 441s), along an across-creek, zig zag pattern from the heads of the GMR and Partings creek to the mouth of the GMR (Fig.1). A waypoint associated depth measurement was taken automatically every 10 seconds during the cruise (average speed 6 knots) as well as manually in areas of interest, for a total of 5942 measurements. A YSI 6600 V2-4 was deployed simultaneously during sampling to record changes in water depth throughout the survey.

Depth measurements taken from the onboard GPS were corrected for transponder location from water surface (10 cm), adjusted for tidal cycle at time of measurement to mean water level on that day, and then adjusted from mean water level on that day to long-term mean sea level at the closest NOAA tide gauge (Wachapreague, VA; NOAA station 8631044). All points from the shoal, channel, and marsh digitization described above were extracted and assigned depths based on the long-term datum at the Wachapreague station: upland marsh edges were defined to be at mean higher high water, upland subtidal shoal edges and marsh islands within shoal segments were defined to be at mean sea level, and channel edges and marsh islands within the channel were defined to be at mean low water. All points were combined and imported into ArcGIS 10.1 and interpolated across the entire GMR system using inverse distance weighting based on natural neighbors with a 5 x 5 m grid resolution. The resulting grid was merged with the model boxes to compute mean depth and volume of each box, and the area of bottom in 0.5 m depth intervals down to 2 m.

III.   *Monthly Water Quality and Dataflow Surveys*

Water quality data for model calibration were collected in collaboration with Dr. Iris Anderson's lab which led a series of water quality and Dataflow surveys in the GMR. Cruises were conducted in along-creek tracks, during ebb tide, from the mouth of the Machipongo to the navigable head waters of the GMR and three tributary creeks. Cruises were conducted monthly, or bimonthly during winter months, on the following dates: June 20, July 23, August 30, September 13, October 16, and November 29, 2012; January 29, March 26, April 24, May 24, and June 25, 2013. The Dataflow system utilizes an on-board YSI 6600 V2 datasonde combined with a pumping system and a GPS unit to associate water quality data with spatial coordinates. The datasonde recorded surface temperature, conductivity/salinity, dissolved oxygen, pH, turbidity, and chlorophyll-*a* (chl-*a*) every 3 seconds during each cruise. All sensors were calibrated against known standards in the lab prior to sampling.

During the surveys, whole water grab samples were taken at the heads and mouths of each creek for laboratory determination of chl-*a*, total suspended solids (TSS), dissolved inorganic nitrogen and phosphorus (DIN/DIP), dissolved organic nitrogen (DON), dissolved organic carbon (DOC), and chromophoric dissolved organic matter (CDOM). Samples were collected in 250 ml brown Nalgene bottles, placed in coolers on ice in the field, and filtered immediately upon returning to the lab. All parameters were filtered and measured in triplicate and averaged, except for CDOM samples which were collected in duplicate.

Whole water samples for chl-*a* analysis were filtered onto Whatman 0.7 μm GF/F filters and frozen for later extraction via the Schoaf and Lium (1976) method, involving

fluorometric readings before and after acidification to correct for phaeophytin content. Whole water samples for TSS were filtered onto Whatman 0.7 μm GF/F filters, dried to a constant weight, weighed, combusted at 550 °C, and weighed again to determine organic content (US EPA 1971). DIN, DIP, and DON concentrations were obtained by filtering whole water samples through 0.45 μm Gelman Supor filters and freezing the filtrate until later analysis on a Lachat autoanalyzer (Smith and Bogren 2001, Liao 2001, Knepel and Bogren 2001); DON required persulfate digestion in sealed ampules prior to analysis (Knepel and Bogren 2001). DIN, DON, and DIP samples were analyzed by Hunter Walker. Whole water samples for DOC analysis were filtered through 0.45 μm Gelman Supor filters and frozen for later analysis on a Shimdazu TOC-V CPH/PN analyzer. Whole water samples for CDOM analysis were filtered through 0.2 μm Nucleopore membrane filters and frozen for later analysis of absorption on a Beckman Coulter DU 800 scanning spectrophotometer.

All YSI data were exported to Excel and quality checks were performed by Jennifer Stanhope. Data spikes, negative readings, and grounding events were identified and data removed. For each dataflow sampling date a regression was fit between YSI chlorophyll readings and extracted chlorophyll values at discrete sampling sites. This relationship was then applied to all YSI chlorophyll readings to calculate extracted values. Each dataflow file was imported into ArcGIS 10.1 and projected onto the delineation of creek boxes, and each parameter was averaged by box.

IV.   *Seasonal Water Quality Measurements*

To quantify diel and tidal excursions of key water quality parameters (salinity, DO) relative to overall gradients within the GMR, and to collect additional data for model calibration, monthly dataflow surveys were supplemented with seasonal sampling efforts, conducted on August 22nd and October 23rd, 2012 and May 9th and July 10th, 2013.YSI 6600 V2 datasondes and/or Hydrolab DS-5X sondes were deployed at the head of Partings Creek (PH), the head of the GMR (MH), and the mouth of the GMR (MM) (Fig 1; Table 2). At PH and MH the instruments were deployed on a dock piling, at a distance of 0.5 m from the bottom, and at MM the instrument was deployed just below mean lower low water on the Great Machipongo Channel Light 8 (CG LL #6920). YSI 6600 V2 data included temperature, salinity, dissolved oxygen, pH, turbidity, and chl-*a*, while Hydrolab data only included temperature, salinity, and dissolved oxygen; all data were collected at 15 minute intervals. All datasondes were calibrated before deployment, and after retrieval quality checks were performed on the data to remove spikes and periods in which the sondes were out of the water.

Additional grab samples for chl-*a*, TSS, DIN, DIP, DON, DOC, and CDOM analyses were taken at PH, MH, and a site midway up the Machipongo (MI). Samples and data were processed as described above. Photosynthetically active radiation (PAR) was measured at PH, MH, and MI using a LiCor LI-1400 datalogger outfitted with 2π quantum sensors. Irradiance data were measured in triplicate above the water surface, just below the surface, and 1 m below the surface and used to calculate the site-specific light attenuation coefficient (k_d).

V.   *Benthic Microalgae*

To quantify the variation in BMA biomass with depth and location within the GMR, samples for benthic microalgae chl-*a* were collected during seasonal sampling at sites PH, MH, and MI as well as spatially during a one-time creek wide survey. A sample of the top 3 mm of sediment was taken in triplicate seasonally, at a consistent depth of 0.5 m below MSL, using a flat tip 5 mL NormJect syringe and placed in 15 mL centrifuge tubes, immediately put on ice in the field, and frozen upon return to the lab. Benthic chl-*a* content of each sample was analyzed per the method of Pinckney and Zingmark (1993) and the equations of Lorenzen (1967). Each sample was thawed, placed in acetone, vortexed for 30 seconds, sonicated for 30 seconds, and extracted in the freezer for 24 hours. Samples were then filtered through HPLC Gelman 0.45 μm CR-PTFE Acrodisc filters and read on a spectrophotometer (Beckman Coulter DU 800) at wavelengths of 630, 664, 665, 647, and 750 nm before and after acidification with 150 μL of 10% HCl to correct for phaeophytin content.

The spatial benthic microalgae survey took place May 9-10, 2014. Sampling locations were selected by dividing the GMR shoreline into 100 m segments in ArcGIS, and then a subset of these segments were selected to sample using a random number generator. A single sample was collected from two depths at each of the 42 sites chosen, except for one site where a single depth was sampled. At each of the 42 sites, the two samples were taken at depths randomly chosen for sampling from 0.25, 0.5, 0.75, 1.0, 1.5, and 2.0 m relative to MSL. Additionally across-creek transects were conducted at the heads of Partings Creek and the GMR with 8 and 6 samples taken respectively across a range of depths. All sample depths were adjusted throughout the sampling day for

current tide stage by consulting the Wachapreague, VA tide chart

(tidesandcurrents.noaa.gov).

VI.   Open Water Metabolism

Net ecosystem metabolism was calculated from the seasonal datasonde

deployments at sites MM, MH, and PH (Fig. 1). NEM was calculated as in Giordano et

al. (2012) from the change in dissolved oxygen per 15-minute time step, integrated over

box segment mean depth and corrected for air-sea exchange (g O_2 m^{-2} 15 min^{-1}) using the

regression of Marino and Howarth (1993) (Eqn. 1):

$$Air - Sea\ Exchange = \left(\frac{e^{1.09+0.249W_{spd}}}{100} \right) * k_{530} * (DO_{sat} - DO_{conc}) * (\Delta t)$$

where W_{spd} is wind speed at 10 m above MSL (m s^{-1}), computed using data from

Wachapreague, VA (NOAA station 8631044), interpolation between points where

missing, and adjusted from the sensor height to 10 m using the equations in Kremer et al.

(2003), DO_{sat} is the dissolved oxygen concentration at saturated conditions (mg l^{-1}),

DO_{conc} is the measured dissolved oxygen concentration (mg l^{-1}), Δt is time interval (0.25

h), k_{530} is transfer velocity coefficient (Eqn. 2):

$$k_{530} = \left(\frac{Sc_{O_2}}{530}\right)^{-\left(\frac{1}{2}\right)}$$

and SC_{O2} is the Schmidt number based on water temperature (T) and salinity (S) (Eqn. 3, Wanninkhof 1992):

$$Sc_{O_2} = 1800.6 + 152.4\left(\frac{S}{35}\right) - T\left(120.1 + 7.9\left(\frac{S}{35}\right)\right) + T^2\left(3.7818 + 0.21\left(\frac{S}{35}\right)\right)$$
$$- T^3\left(0.047608 + 0.002483\left(\frac{S}{35}\right)\right)$$

Computed values of NEM for each 15 minute interval were summed over each day to obtain an estimate of daily NEM, and daily rates were averaged across each deployment.

VII. *Component Metabolism*

Component incubations were used to quantify net metabolism of the water column and sediments seasonally at sites PH, MH, and MI following the approach of Giordano et al. (2012) and Lake et al. (2013). Whole water was collected in duplicate in dark 4 l bottles for water column incubations, with an additional 40 l of site water collected for use in sediment incubations. Thirty sediment cores were collected at each site using a PVC pole corer at an approximate depth of 0.5 m below mean sea level. Each acrylic core had a height of 15 cm and internal diameter of 4.1 cm, and each sample had an average sediment height of 7 cm with 8 cm of overlying water. Sediment cores were

capped, and all cores and whole water samples for incubation were placed in coolers with a mix of ambient water and ice and taken back to the lab.

Water column incubations were conducted immediately after returning from the field. Duplicate photosynthesis-irradiance (P-I) curves were developed for each site by incubating 10 water column samples from each collection bottle across a range of light levels in 60 ml Biological Oxygen Demand (BOD) bottles at ambient temperature for less than 3 hours. Similarly, duplicate sets of three dark bottles were incubated for each site overnight (approximately 12 h) to measure respiration. PAR levels in the light gradient box were measured before incubations using a LiCor LI-1400 datalogger outfitted with a 2π quantum sensor. DO concentrations were measured before and after incubation using a Hach HQ 40d DO meter with LDO optical probes. LDO probes were calibrated in water-saturated air before each use.

Upon returning from the field, sediment cores were uncapped and allowed to equilibrate to ambient conditions overnight in a gently stirred bath of site water. The next day cores were carefully drained of overlying water, replaced with filtered site water (0.45 µm), capped with polyethylene (Saran Wrap^{TM}) which has a low oxygen permeability of 5.8×10^{-5} ml cm^{-2} h^{-1} (Pemberton et al. 1996), and incubated as for water samples at ambient temperature for less than three hours for light cores (two duplicate sets of 10 cores per site) and less than five hours for dark cores (two duplicate sets of three cores per site). Immediately following sediment incubations, a subsample of the top 3 mm of sediment was taken from each core for analysis of chl-*a* concentration as described above.

Production and respiration were calculated for the light and dark samples, using the change in oxygen concentration in each sample over the incubation period, and normalized to field chlorophyll-*a* concentrations (water column) and benthic chlorophyll-*a* concentrations measured in each incubation core (sediment). Curves were then fit to the production vs. irradiance data in SAS 9.2 to produce two P-I curves per site per season, for a total of 24 water column and 24 sediment curves (Fig. 3). Water column P-I curves were fit with the Platt et al. (1980) function (Eqn. 4), which accounts for photoinhibition:

$$P^B = P_s^B \left(1 - \exp\left(1 - \frac{\alpha^B I}{P_s^B} \right) \right) * \exp\left(-\frac{\beta^B I}{P_s^B} \right) - R^B$$

Sediment P-I curves were fit with the Jassby and Platt (1976) function (Eqn. 5), which does not include photoinhibition:

$$P^B = P_{max}^B \tanh\left(\frac{\alpha^B I}{P_{max}^B} \right) - R^B$$

where P^B is the biomass normalized photosynthetic rate (mg O_2 mg chl^{-1} h^{-1}), P^B_s is the biomass normalized maximum photosynthetic rate in the absence of photoinhibition (mg O_2 mg chl^{-1} h^{-1}), P^B_{max} is the biomass normalized maximum photosynthetic rate (mg O_2 mg chl^{-1} h^{-1}), α^B is the initial slope of the P-I curve (mg O_2 mg chl^{-1} h^{-1}(μE m^{-2} s^{-1})$^{-1}$), I is irradiance (μE m^{-2} s^{-1}), β is the photoinhibition parameter (mg O_2 mg chl^{-1} h^{-1}(μE m^{-2} s^{-1})$^{-1}$), and R^B is biomass normalized respiration (mg O_2 mg chl^{-1} h^{-1}).

Duplicate P-I curve parameters were averaged at each site and used to calculate hourly production and respiration in 10 cm depth bins using site specific k_d and hourly irradiance (photosynthetically active radiation, PAR) from the Virginia Coast Reserve Long-Term Ecological Research (VCR-LTER) site at Oyster, VA. Hourly PAR was averaged over the month of each measurement to avoid undue influence by particularly cloudy days when they coincided with sampling. Biomass specific rates from the P-I calculations were converted to volume- and area-specific rates using field measurements of water column and benthic chl-*a* concentrations, respectively. Daily water column and sediment GPP and R were scaled to areal rates using creek box depth. Daily NCP was computed as GPP - R and water column and sediment NCP were summed to obtain an independent daily estimate of NEM.

Great Machipongo River Ecosystem Model (GMR-EM)

A mechanistic, reduced complexity, management-relevant model was applied to the GMR that simulates state variables and processes of first-order importance to estuarine eutrophication, with a core set of key rate processes (phytoplankton production, pelagic respiration, and carbon flux to the sediments) formulated using robust, cross-system empirical relationships shown to apply across a wide range of temperate estuaries and rooted in actual measurements (e.g., ^{14}C or O_2 production), allowing direct comparison of model predictions to observations (Fig. 2) (Brush 2002, 2013, 2015; Brush et al. 2002; Lake & Brush 2015). An important distinction is made in the model between water column and benthic production and respiration, which will identify their relative

importance in nutrient processing and as 'filters' in the system.

The model simulates daily fluctuations over an annual cycle of phytoplankton and BMA biomass (as C, N, P, and Chl-*a*), water column DIN, DIP, dissolved oxygen (O_2), and labile carbon and associated nutrients, and sediment organic carbon and associated nutrients (Fig. 2; Brush 2013; Brush and Nixon 2010; Lake and Brush 2015). The coarse spatial resolution of the EEM has the advantage of rapid implementation in new study systems, fast run times (seconds to minutes) on desktop PCs, operation at the typical scale of monitoring data, and ready translation to a user-friendly, decision-support tool directly usable by resource managers. This approach is in line with recent calls for management-relevant models of intermediate complexity as an alternative to more complex, highly parameterized models (e.g., NRC 2000; Duarte et al. 2003), and recent work has confirmed the utility of simplified boxed approaches (e.g., Menesguen et al. 2007; Testa and Kemp 2008).

The EEM has been applied to Hog Island Bay and the lagoons along the entire Delmarva Peninsula as part of Virginia Sea Grant project R/715165, and was expanded to capture the nutrient dynamics in the GMR creek system using site specific data collected during this project. The model was run for a period of one year to encompass the annual cycle of water quality and Dataflow monitoring along with seasonal sampling (see above), from 6/26/2012 to 6/25/2013, and was solved using the Runge-Kutta method at a time step of 0.03125 d.

I.   *Spatial Elements and Physical Exchanges*

The model was run in the five boxes defined above, which were assumed to be vertically well-mixed, with the following exchanges among boxes: MH <-> MSB, MSB <-> MI, MI <-> MM, PH <-> MM, and MM <-> Hog Island Bay (Fig. 1). Volume exchanges in the EEM were initially calculated using both one dimensional Officer box model (1980) and tidal prism approaches. The Officer box model uses freshwater input and a salt balance between each box to calculate exchanges (Officer 1980). The tidal prism method is a way of calculating flushing time that works best for shallow systems, with low freshwater inputs and large tidal ranges like the tidal creeks on the Virginia Eastern Shore (Monsen et al. 2002; Herman et al. 2007). We compared the modeled results using each approach to measured results and found the tidal prism approach produced more reasonable results. We believe this is due to the small differences in salinity between each box, which limits the ability of the Officer approach to compute fluxes. After these comparisons were performed, we chose to use the tidal prism method to calculate volume exchanges across each boundary from box surface area and the 1.23 m mean tide range at Wachapreague, VA, assuming two flooding and two ebbing tides per day. BMA were simulated in the following depth intervals: 0-0.5, 0.5-1, 1-1.5, 1.5-2, and greater than 2 m.

II.   *Forced Data*

Watershed nitrogen inputs for the model were provided by a spreadsheet-based Nitrogen Loading Model (NLM), originally developed by Valiela et al. (1997), adapted to Chincoteague Bay, MD/VA by Cole (2005), applied to selected watersheds on the

Virginia Eastern Shore by Giordano et al. (2011), and applied to the seaside watersheds along the entire Delmarva Peninsula including Hog Island Bay by Brush et al. (2015). The NLM is a spreadsheet-based model which computes mean annual total nitrogen (TN) loading given estimated or measured annual nitrogen inputs onto different land use types, human and animal populations, and attenuation by lumped terrestrial biogeochemical rate processes. Total load (4.6 kg ha^{-1} y^{-1}; including groundwater) was prorated to each box watershed based on area. Watershed phosphorus loading to the system was calculated using the TN loads from the NLM combined with measured TN: PO4 ratios (436 g g^{-1}) of three headwater streams in the GMR system (Machipongo, Partings, Greens; Stanhope et al. 2009). An average watershed dissolved organic carbon load of 3.7 (kg C ha^{-1}y^{-1}) was also obtained from a previous study of baseflow nutrient analysis in the three headwater streams (Stanhope et al. 2009). Direct atmospheric N deposition was obtained from the calculation of direct atmospheric deposition in the NLM, which uses a value of 6.2 kg ha^{-1} y^{-1}, while atmospheric P deposition was assumed to be zero (Brush et al. 2015).

Box averages from the dataflow cruises provided annual cycles of daily water temperature (°C), salinity, and turbidity (NTU) via linear interpolation between cruise dates. Meteorological data were forced using data from local stations where available. An annual cycle of average daily wind speed (m s^{-1}) was obtained from Wallops Island, VA (NWS 724020) and Wachapreague, VA (NOAA station 8631044) where there were data gaps. Average daily air and dew point temperature (°C) were obtained from Accomack Airport (NWS 724026) and Wallops Island, VA (NWS 724020) where there were data gaps. An annual cycle of total daily precipitation was obtained from Painter,

VA (USC00446475; NWS 490303). An annual cycle of total daily PAR was obtained

from Taskinas Creek, VA (National Estuarine Research Reserve site CBVTCMET).

Boundary conditions at the mouth of the system for salinity and DO were obtained

from the portion of monthly dataflow surveys that extended beyond the model domain,

and DIN, DIP, chl-*a*, and water column DOC were obtained from the monthly discrete

samples taken closest to the mouth of the system in lower Upshur creek (UM; Fig. 1).

All values were linearly interpolated between sampling dates.

III. *Model Parameterization and Calibration*

Light attenuation was calculated using a regression of measured k_d (m^{-1}) with

observed chl-*a* concentration (ug l^{-1}) and turbidity (NTU):

$$k_d = 1.012 + (0.109 * \text{chl-}a) + (0.041 * \text{NTU}) \qquad R^2 = 0.504$$

In the absence of site-specific data for the carbon to chlorophyll-*a* ratio of phytoplankton

and benthic microalgae, the value used for both autotrophs was taken as the slope of a

regression between particulate organic carbon and chlorophyll-*a* using multiple years of

monitoring data from the EPA Chesapeake Bay Program (64 g g^{-1}; Brush, unpublished).

The reduced complexity nature of the model results in a limited number of tuning

parameters for calibration. Calibration parameters in the model included the zero-degree

intercept and exponent of the temperature dependent functions for water column and

sediment respiration and denitrification, and coefficients for the BMA loss terms. These

parameters were adjusted to calibrate the model to match observed concentrations of

water column and benthic chlorophyll-a, DIN, DIP, and DO, and measured rates of water

column and sediment GPP and R from the component incubations.

Once calibrated the model was used to create annual nutrient budgets by box and

for the entire system. The budget for the entire system was used to assess the role of the

GMR in transporting, transforming, or filtering watershed-derived nutrients by

comparing nitrogen inputs from the watershed, atmosphere, and Hog Island Bay to

internal processing and losses through phytoplankton uptake, benthic microalgal uptake,

denitrification, and export to Hog Island Bay. The budgets for each box were used to

assess the relative importance of these internal processes along the watershed to bay

gradient. The model was also used to simulate a storm event that occurred during the

study period. The nutrient budget from the storm simulation was then compared against

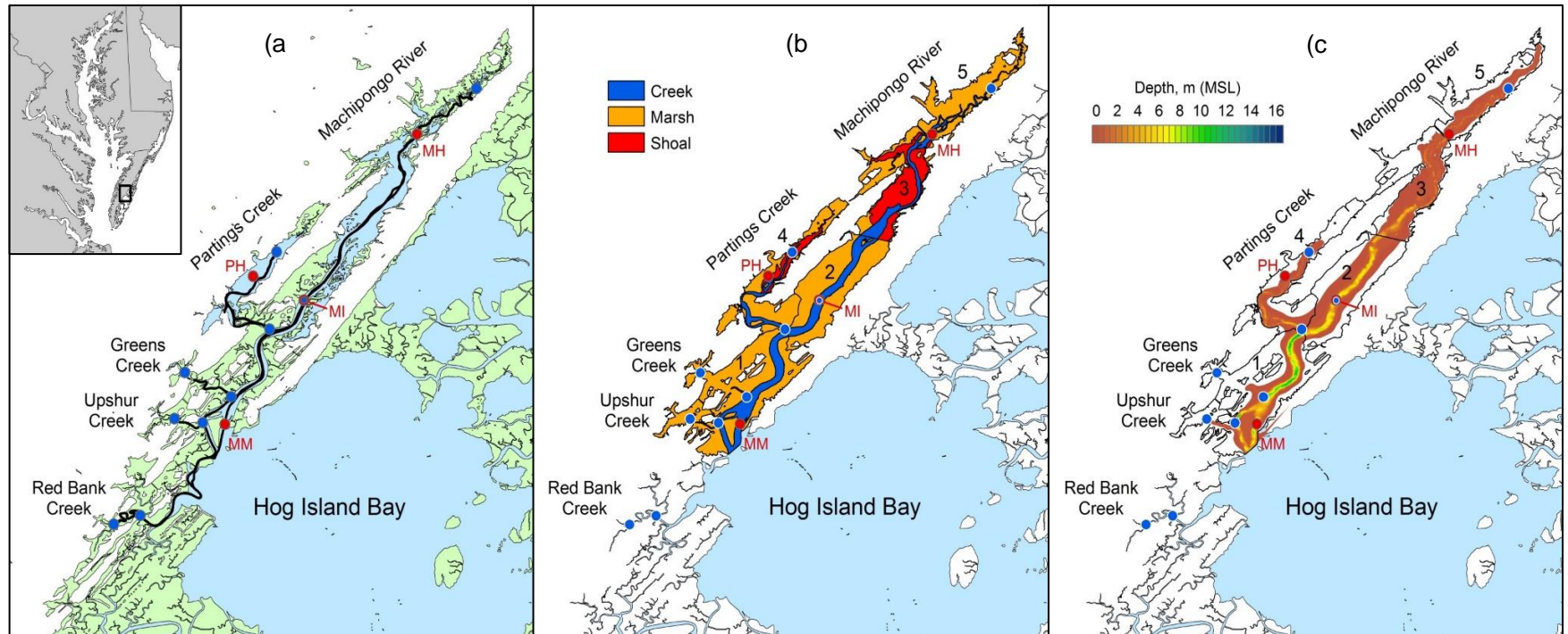the budget from the baseline model run.

Figure 1: Hog Island Bay and the Great Machipongo River system (GMR) (Inset: The Virginia Eastern Shore). Seasonal sampling sites for metabolism studies are in red- Machipongo Head (MH), Partings Head (PH), and Machipongo Mouth (MM). Grab sample sites as part of the monthly dataflow cruises are in blue. Site Machipongo Intermediate (MI) is both a seasonal and grab sample site and is outlined in red and filled in with blue.
(a) A typical dataflow track through the GMR with open water in blue and intertidal marshes in light green, base layer-NHD high resolution database. (b) The GMR delineated for creek, shoal, and marsh regions within each box 1-5. (c) Interpolated bathymetry of the GMR based on our system depth survey-used for model calibration.
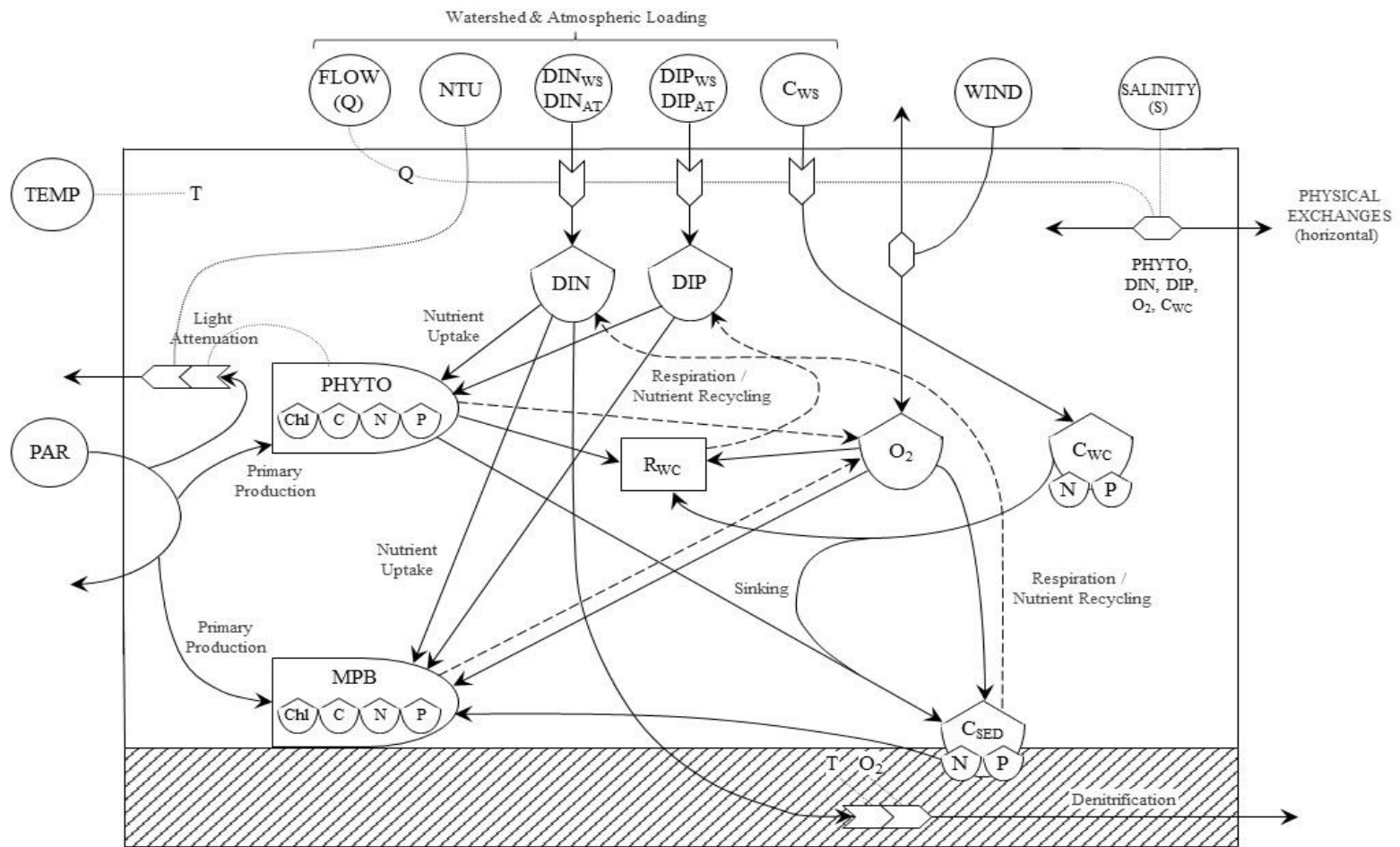
Figure 2: Great Machipongo River-Estuarine Ecosystem Model (GMR-EEM) (modified from Brush 2002; Brush and Harris 2016)
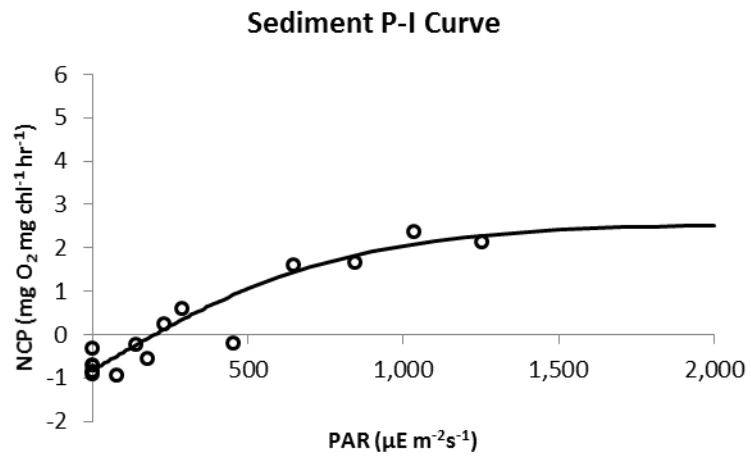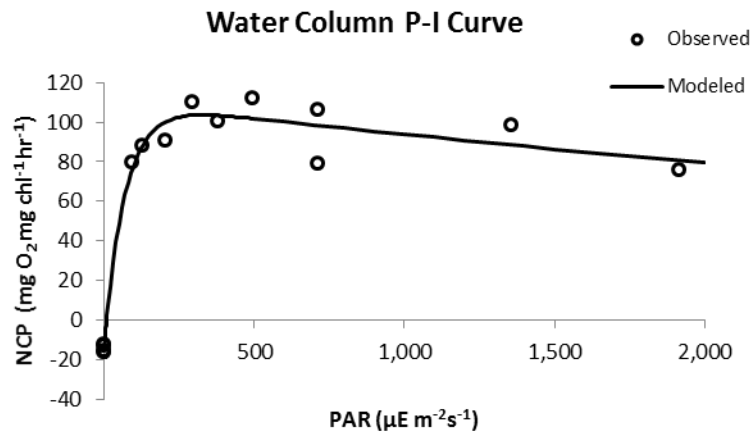
Figure 3: Example P-I curves taken from MH Spring 2013 sampling for Water Column (top) and Sediment (bottom) incubations

Table 1: Creek Box Dimensions and Characteristics

Creek Box	Creek box area (m²)	Watershed Area (m²)	Volume (m³)	Tidal Prism volume (m³)	Mean depth (m)	Max Depth (m)	Mean Salinity (ppt)
1	3,458,800	16,517,257	7,669,245	4,254,324	2.22	16.0	30.3
2	3,507,425	4,859,006	4,384,438	4,314,132	1.25	8.7	28.8
3	3,434,675	14,170,676	2,202,718	4,224,650	0.64	6.3	26.6
4	2,138,475	20,766,180	1,161,073	2,630,324	0.54	8.5	28.1
5	1,736,075	37,948,500	862,815	2,135,372	0.50	6.3	24.1

Table 2: Seasonal YSI and Hydrolab deployment schedule

	Late Summer 2012		Fall 2012		Spring 2013		Early Summer 2013	
	YSI	Hydrolab	YSI	Hydrolab	YSI	Hydrolab	YSI	Hydrolab
PH	8/22-30			10/16-31		5/9-21		6/25-7/6
MH	8/22-30		10/16-11/5		5/9-24		6/25-7/9	
MM	8/22-26			10/16-27	5/9-24		6/25-7/10	

RESULTS

Metabolism Results

Component Metabolism by Season

Water column GPP was greatest at MI, followed by MH and then PH for all seasons except fall when all sites experienced extremely low rates and GPP at MI was zero (Fig 4a-c). All sites followed a seasonal pattern of decreased water column GPP in fall, elevated rates in spring, and highest rates in early summer (Fig 4a-c). Late summer water column GPP was higher than fall GPP at all sites, with the largest difference at MI (Fig 4a-c).

Sediment GPP was highest at PH, followed by MH and then MI for all seasons except late summer when the pattern reversed (Fig 4d-f). MH sediment GPP was highest in spring, but showed very little seasonality (Fig 4d). PH sediment GPP was highest in early summer and 2.5-7 times higher than rates at any other site during any season (Fig 4d-f). MI sediment GPP was very low except for the late summer sampling, when it was similar to rates experienced at the other sites (Fig 4f).

Rates of water column respiration were low, less than $1\ g\ O_2\ m^{-2}\ d^{-1}$, across all sites and dates. MI water column respiration was the highest for all seasons except fall when MH had the highest rate (Fig 4a-c). Water column respiration was lowest during fall (Fig 4a-c). Sediment respiration rates were highest at site MH except for early summer when PH experienced very

high sediment GPP and respiration (Fig 4d-f). All sites experienced similar rates of sediment respiration in late summer, fall, and spring with the lowest rates in fall (Fig 4d-f). Early summer sediment respiration decreased from spring at sites MH and MI but increased substantially at site PH (Fig 4d-f).

Water column GPP exceeded sediment GPP on all dates at MI and half the time at MH, while sediment GPP was higher on all dates at PH (and half the time at MH) (Fig 4). With the exception of one date at MI, sediment respiration was always greater than water column respiration across all sites (Fig 4). Water column NCP was positive, net autotrophic, for all sites and seasons except for MI during fall, when it was zero (Fig 4a-c). All sites experienced the lowest water column NCP in fall and the highest in early summer (Fig 4a-c). While all sites displayed similar temporal patterns of sediment NCP, rates were not consistently positive or negative (Fig 4d-f).

Combining water column and sediment rates, all sites were net autotrophic (positive NEM) for all dates except late summer when MH and PH were net heterotrophic (negative NEM), and fall when NCP at MI was balanced (Fig 5a-c). All sites experienced a large increase in NEM during early summer (Fig 5a-c), and PH also displayed a large increase in autotrophy in the fall (Fig 5b).

Component Metabolism: Overall Averages

The preceding patterns were also reflected in average rates across all seasonal samplings (Fig 6). MI had the highest average water column GPP, respiration, and NCP, while PH had the highest average sediment GPP, respiration, and NCP (Fig 6a, d). Average water column NCP was positive (net autotrophic) at all sites, while sediment NCP was mixed (Fig 6a, d).

Sediment GPP and respiration were dominant at the two sites near the head of the system (MH, PH), while pelagic GPP and respiration were dominant mid-system (MI) (Fig 6b, e). The benthic to pelagic GPP ratio at the mid-system site was less than one, indicating pelagic production was more important at this site (Fig 6b), while the benthic to pelagic respiration ratio was 0.98, indicating the rates were approximately equal (Fig 6e). Benthic to pelagic ratios of GPP and respiration were greater than 1 at the headwater sites, indicating the dominance of benthic metabolism at these sites, particularly respiration (Fig 6b, e).

All sites were net autotrophic on average, with system production to respiration ratios greater than 1 (Fig 6c, f). PH was the most autotrophic followed by MI with MH experiencing the lowest net autotrophy (Fig 6c). Autotrophy at PH appeared to be driven by the highest levels of sediment GPP while autotrophy at MI was driven by the highest rates of water column GPP (Fig 6a, d). NEM at MH was driven by a more balanced ratio of water column to sediment GPP (Fig 6a, d).

Open Water Metabolism and Comparison to Component Rates

Net Ecosystem Metabolism as calculated using the open water method was negative (i.e., net heterotrophic) at all sites during all seasons (Fig 7). The largest heterotrophic rates occurred during late summer at sites MH and PH with the lowest rates occurring at site MM (Fig 7). During fall, spring, and early summer all sites experienced similar rates of heterotrophy except for a larger rate at PH during early summer (Fig 7). Open water NEM was in direct opposition to component NEM for all sites and seasons except late summer at sites MH and PH, where both methods indicated net heterotrophic conditions albeit not of the same magnitude (Fig 8).

Modeling Results

Pelagic State Variables

The model captured the seasonality of water column chlorophyll-*a* concentrations in all boxes, exhibiting a bloom in spring and elevated concentrations throughout the summer (Fig 9a). In the upstream boxes 3-5 the model underpredicted water column chlorophyll-*a* during the blooms, with the most pronounced difference between modeled and observed values in box 5 (Fig 9a). Modeled DIN concentrations followed the seasonal trends in observed concentrations, with peaks in late-August through mid-September, mid-November, and late spring/early summer (Fig 9b). To varying degrees, data from all boxes exhibited elevated DIN concentrations in late August through September that the model did not fully capture (Fig 14b; see below). Similarly unexplained peaks in observed DIP concentrations occurred in boxes 2-5 concurrently with the DIN peaks (Fig 9c). DIP concentrations were slightly underpredicted in all boxes except box 1, although the model captured the correct seasonality (Fig 9c). The model also captured the seasonality and magnitude of DO concentrations, although it did not fully reproduce a drawdown of DO in summer months in boxes 2-5 (Fig 10a).

Metabolic Rates

The model computes daytime phytoplankton net primary production (NPP) which is somewhere between GPP and NCP as observed in the metabolic incubations, so model output was compared to both. Modeled phytoplankton NPP followed the observed seasonality in

measured rates, but underpredicted spring and late summer magnitudes (Fig 10b). Modeled

water column respiration followed the overall seasonality of measured rates, but slightly

overpredicted their magnitude (Fig 10c).

Measured sediment GPP is from samples taken from a depth of 0.5 m. Since the model

calculates BMA GPP in 0.5 m depth bins, model output from the 0-0.5 and 0.5-1 m intervals was

compared to the observations (Fig 11a); modeled rates in these two layers should bracket the

observed rates. Modeled sediment GPP was in the appropriate range except for an

underprediction in fall in box 4. Modeled sediment respiration matched well with the observed

rates in fall, and while overall the model demonstrated the correct seasonality, it

underestimated the rates in late summer and spring (Fig 11b). Modeled denitrification (DNF)

followed the simulated pattern of DIN (Fig 11c). DNF rates were not measured in the GMR

system for this study, but modeled values lie in the range of rates measured previously in HIB

(Anderson et al. 2010; Anderson, unpub. data).

Benthic Microalgae

Due to the importance of BMA in shallow systems and their patchy nature, two

approaches were utilized to ensure the model was predicting BMA chlorophyll-*a* concentrations

correctly. The seasonal BMA samples collected at 0.5 m were used to calibrate modeled

concentrations from the 0-0.5 m and 0.5-1 m depth bins (Fig 12). The randomized BMA survey

in May 2014 was used for comparison to model predictions averaged for the month of May

2013 (Fig 13). While this is not a direct comparison, the values should be within the same

approximate range.

The model captured the overall magnitude of observed BMA chl-*a* concentrations from the seasonal sampling, although it failed to match the late summer peak in box 2 and the fall peak in box 4 (Fig 12). Modeled BMA chl-*a* concentrations for May of the model run also fell within the range of observed values from the systemwide survey in the shallowest three depth bins, albeit at the lower end of the range (Fig. 13). The model underpredicted BMA chl-*a* in the deepest depth bins.

Storm Simulation

Late summer and fall 2012 YSI and Hydrolab deployments occurred during storm events (Fig 14). The event during the late summer deployment was characterized by rainfall of 14.5 cm in one day, August 25th, and the fall event was the passage of Hurricane Sandy on October 27-30th, characterized by 7.19 cm of rainfall. In the headwaters of the Machipongo, Hurricane Sandy caused reduced salinity, a spike in turbidity lasting 3 days, an increase in chlorophyll-*a* concentrations, and a dampening effect on dissolved oxygen fluctuations (Fig 14).

The timing of the late summer storm event coincided with the peaks in observed DIN and DIP concentrations and the minimum in observed DO that were unexplained by the model output (Figs 9b, c and 10 a). Since the baseline model uses constant rates of watershed loading, we hypothesized that increased loading during the storm would account for the observed peaks in DIN and DIP.

To attempt to match the model output to the observed peaks, we ran a storm simulation in the model. Watershed loads of N, P, and C were increased for a period of 11 days surrounding the storm; the degree of increase was tested by sensitivity analysis until modeled DIN and DIP concentrations matched observed values. The storm simulation captured the late

summer peak observed in DIN with the addition of this storm, and rates of DNF slightly

increased (Fig. 15). The addition of the storm did not affect the output for any other variables.

System Nutrient Budget

Model output from the baseline calibration and the storm simulation were used to

develop annual nitrogen budgets to assess the role of the GMR as a conduit, transformer, or

filter of land-based nutrient inputs. Inputs to the system under the baseline simulation were

greatest from net exchange with Hog Island Bay, with combined watershed and atmospheric

loads representing less than half the HIB input (Table 3). Atmospheric deposition was the

lowest source of N to the system, at 20% of the input from the watershed, unlike in Hog Island

Bay where atmospheric deposition accounted for 66% of total inputs (Anderson et al. 2010).

Regarding the exchange with HIB, N was imported in inorganic form and exported in

phytoplankton biomass. However, these values only account for DIN and phytoplankton N; the

model does not simulate DON which if included could presumably modify or reverse this net

flux.

Internal processing of N was dominated by BMA uptake, followed by phytoplankton

uptake and a much lower removal by DNF (Table 3). Uptake by BMA and phytoplankton were

balanced near the mouth of the GMR, with increasing dominance by BMA uptake towards the

shallower, upstream boxes. Denitrification was most important near the mouth, and decreased

upstream. On an annual basis, phytoplankton, BMA, and DNF were predicted to uptake or

remove 260%, 413%, and 46% of watershed TN inputs and 69%, 110%, and 12% of all combined

TN inputs from the watershed, atmosphere, and Hog Island Bay.

The August storm simulation added a total of 28,635 kgN y^{-1} to the system from the watershed (Table 4). This nitrogen was mostly flushed from the system to Hog Island Bay, reflected in a reduced net import of DIN, with a small portion being denitrified within the system. Other processes in the budget barely changed or did not change at all, which corresponds with unchanged model output for all parameters other than DIN and DNF.
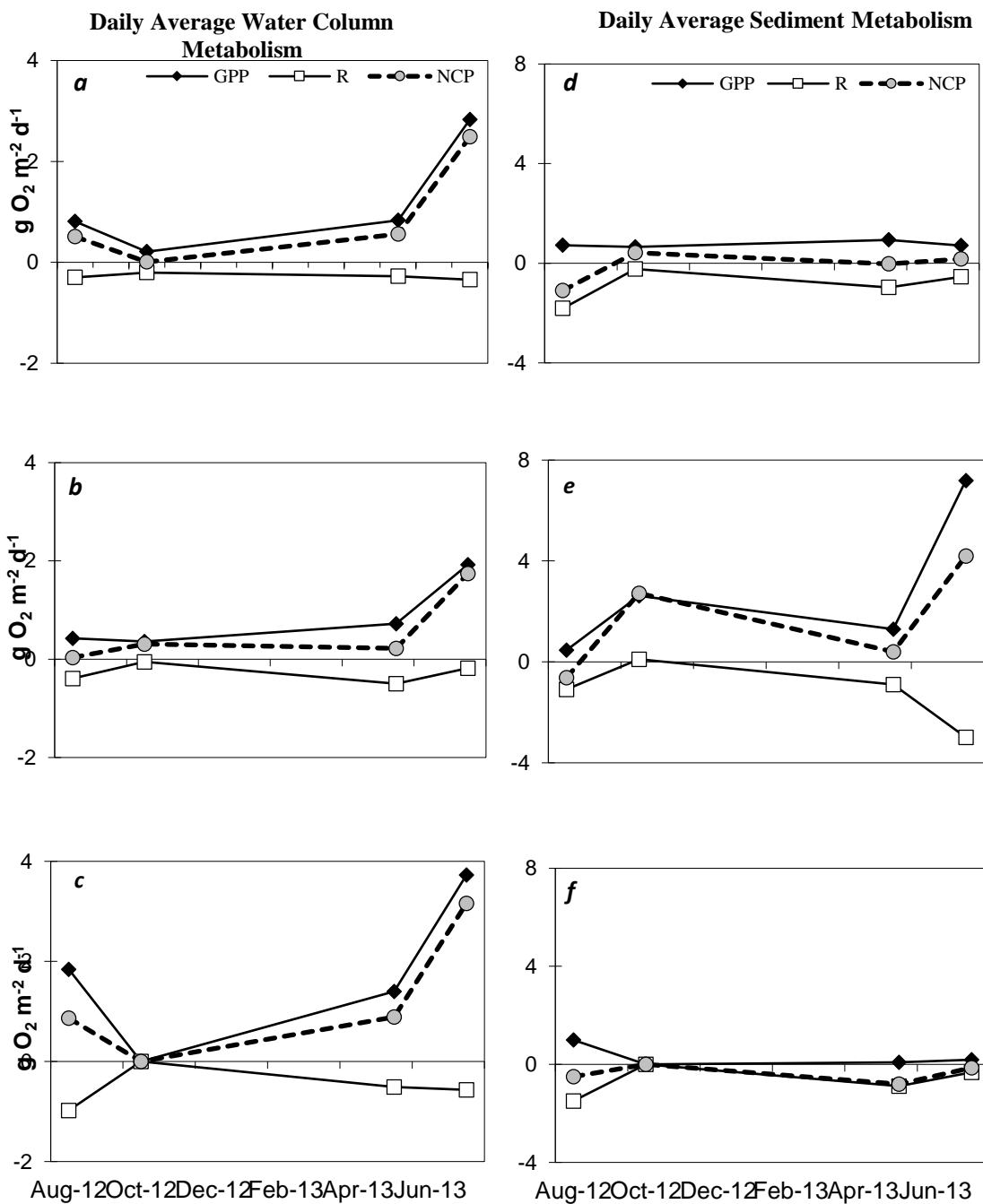
Figure 4: Daily Average Metabolic Rates by site: MH (a., d.), PH (b., e.), and MI (c., f.). Daily Average Water Column GPP, R, and NCP (a.-c.) and Sediment GPP, R, and NCP (d.-f.) (note different scales of water column and sediment rates)

Daily Average NEM

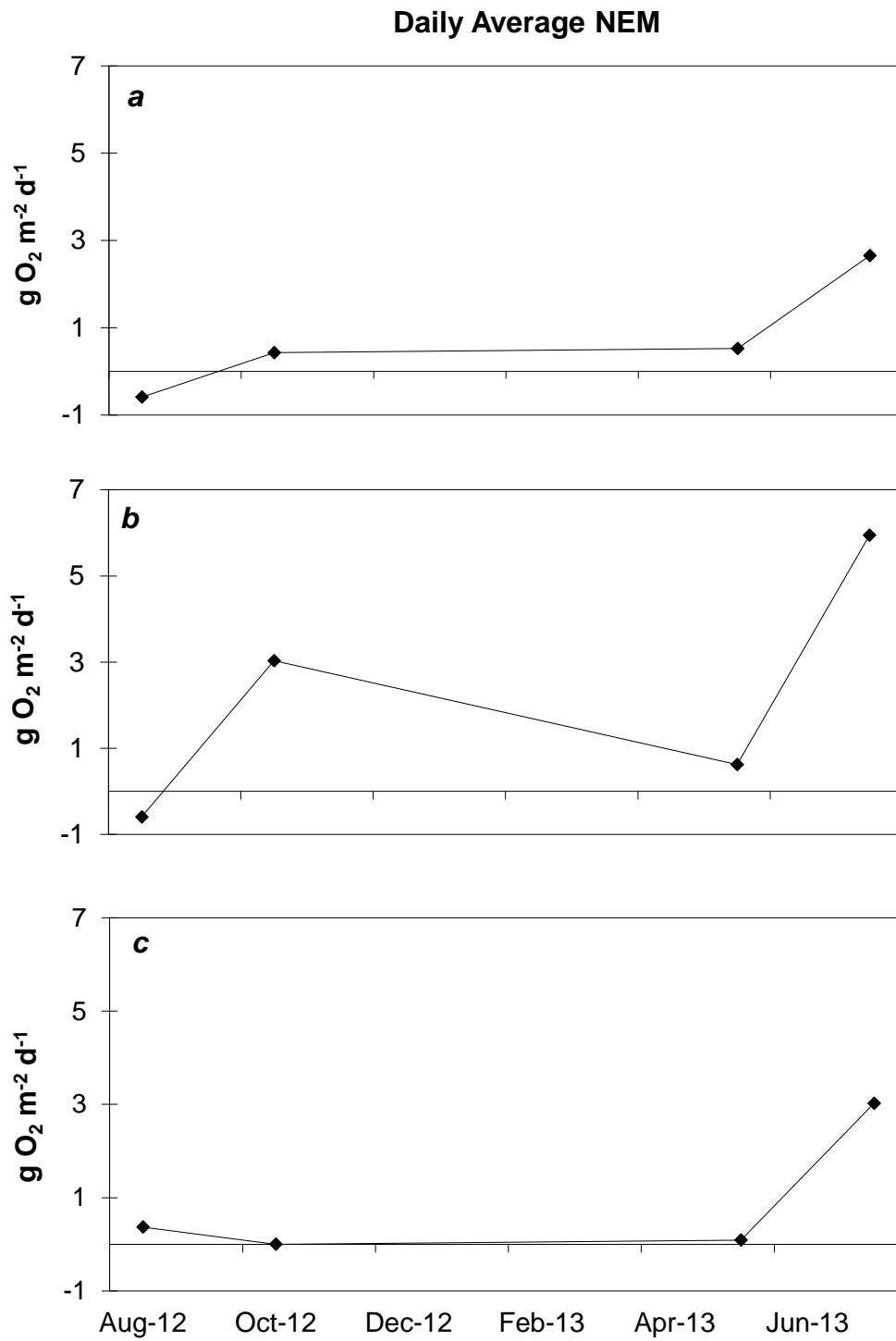Fig 5: Daily average Net Ecosystem Metabolism
using the combined component method at sites MH
(a.), PH (b.), and MI (c.)
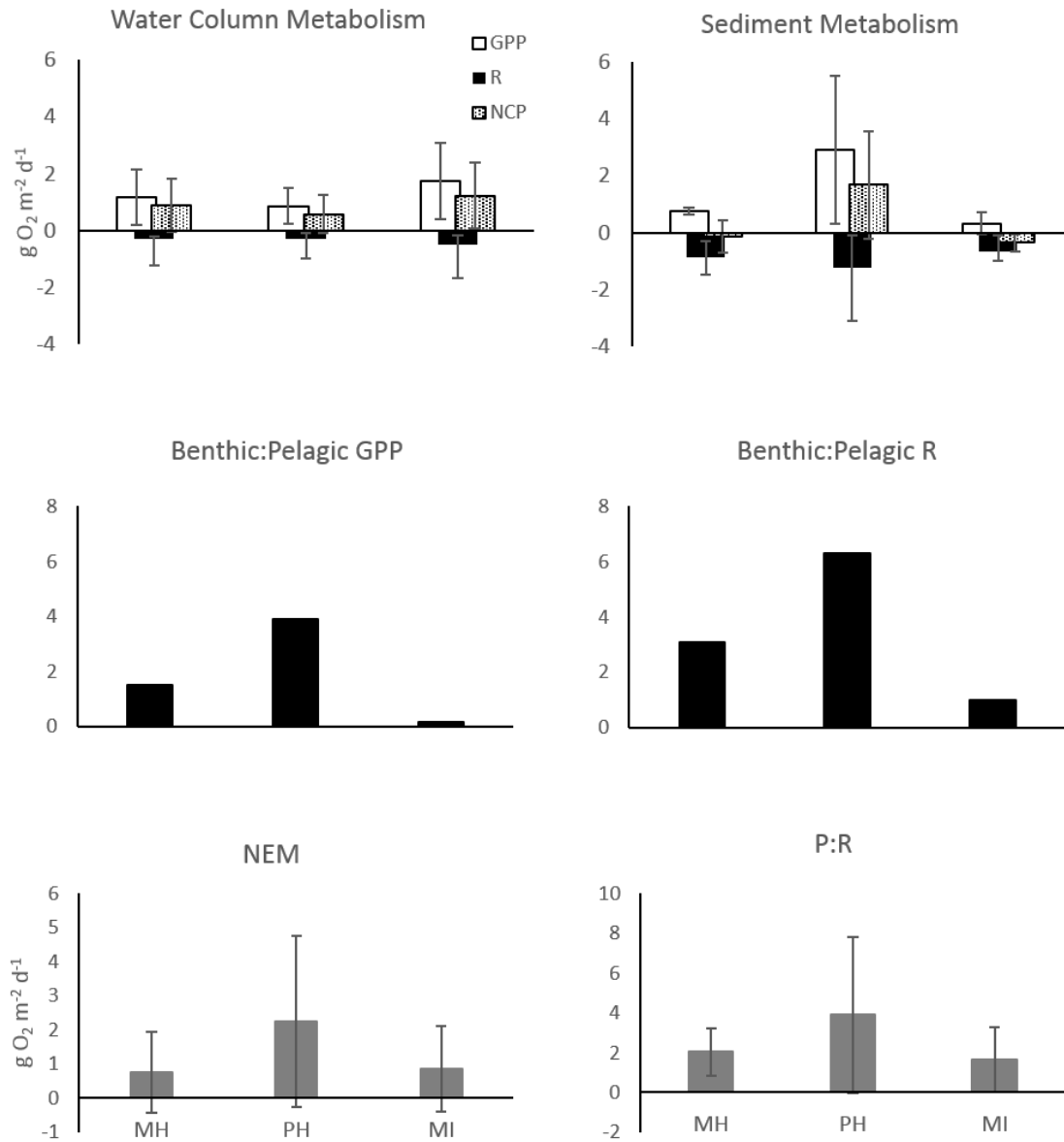
Figure 6: Cross site comparisons of: Water Column and Sediment metabolic rates (a., d.), Benthic to Pelagic Ratios of GPP (b.) and R (e.), Net Ecosystem Metabolism (c.), and Production to Respiration (f.). Error bars represent standard deviation of the average across all 4 seasons at each site.
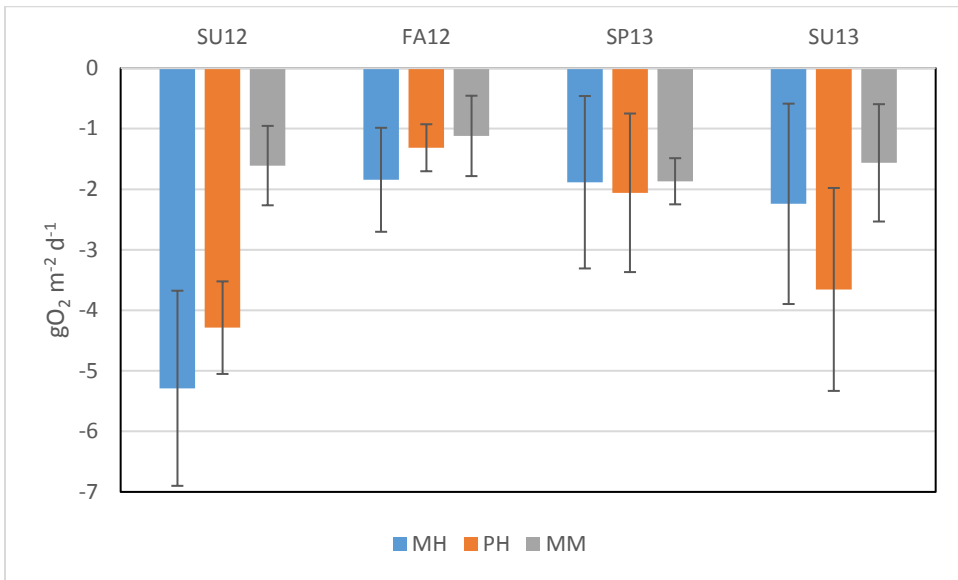
Figure 7: Open water NEM comparison of all sites MH, PH, and MM for 4 seasonal sampling dates, error bars represent standard deviation across all daily rates for the deployment.
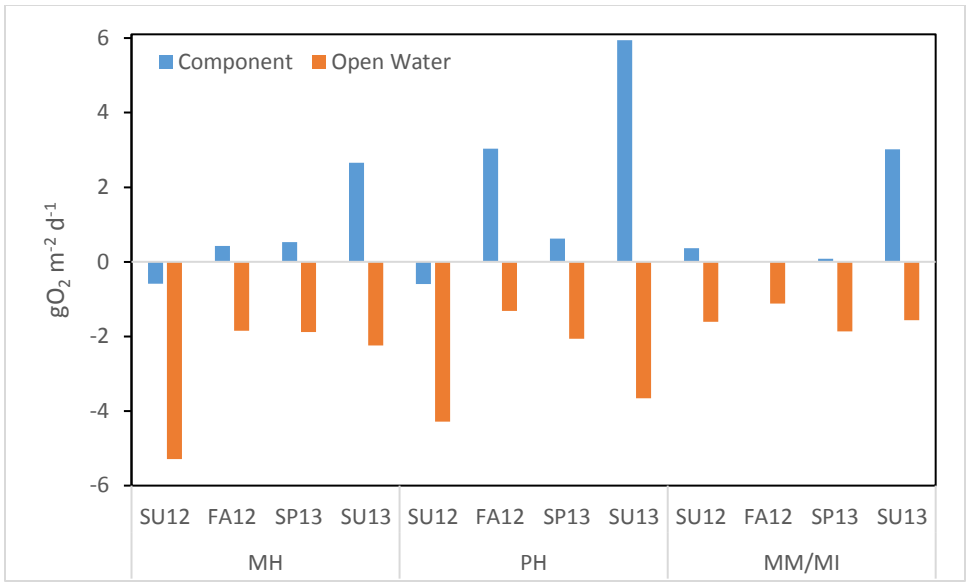
Figure 8: Open water vs. component NEM of all sites MH, PH, and
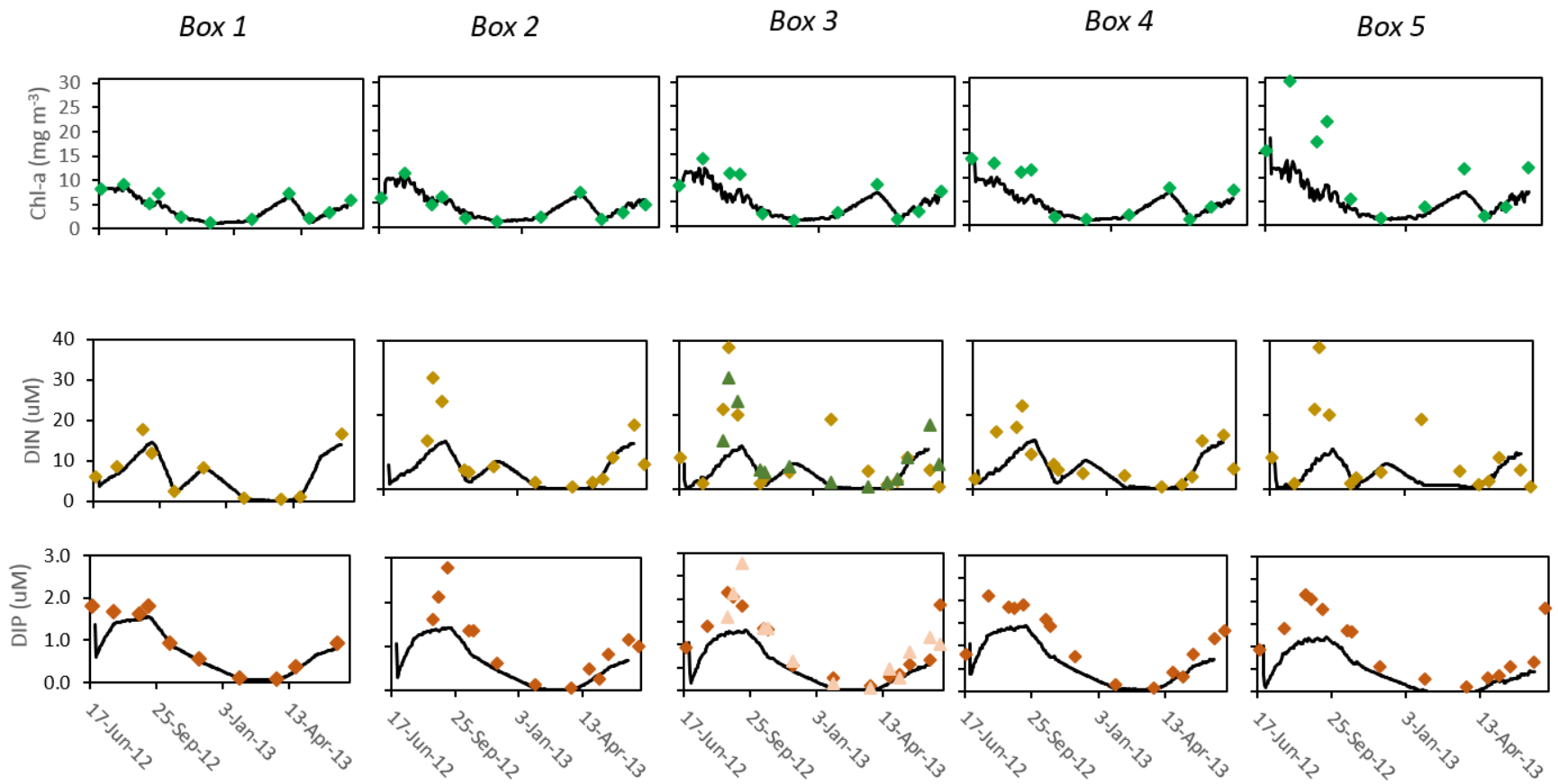
Figure 9: Measured (diamond and triangles) and modeled (black lines) Chlorophyll-a, DIN, and DIP concentrations. Box 3 measured data is from the box upstream (box 5: diamonds) and downstream (box 2: triangles) as there was no data collected at this site for comparison.
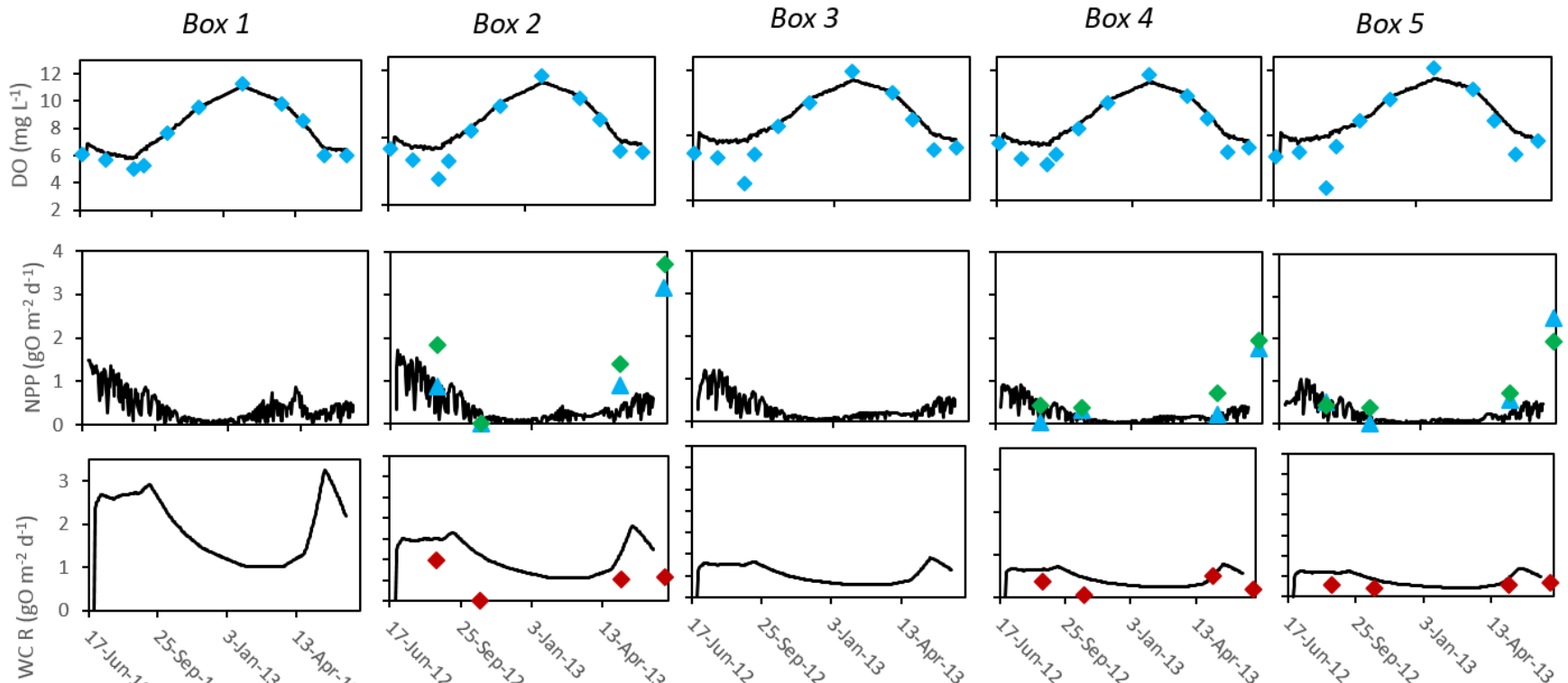
Figure 10: Measured (diamonds) and modeled (black lines) Dissolved Oxygen concentration, Water Column NPP rates, and Water column R rates. Data for calibration of water column NPP are water column GPP (diamonds) along with water column NCP (triangles)
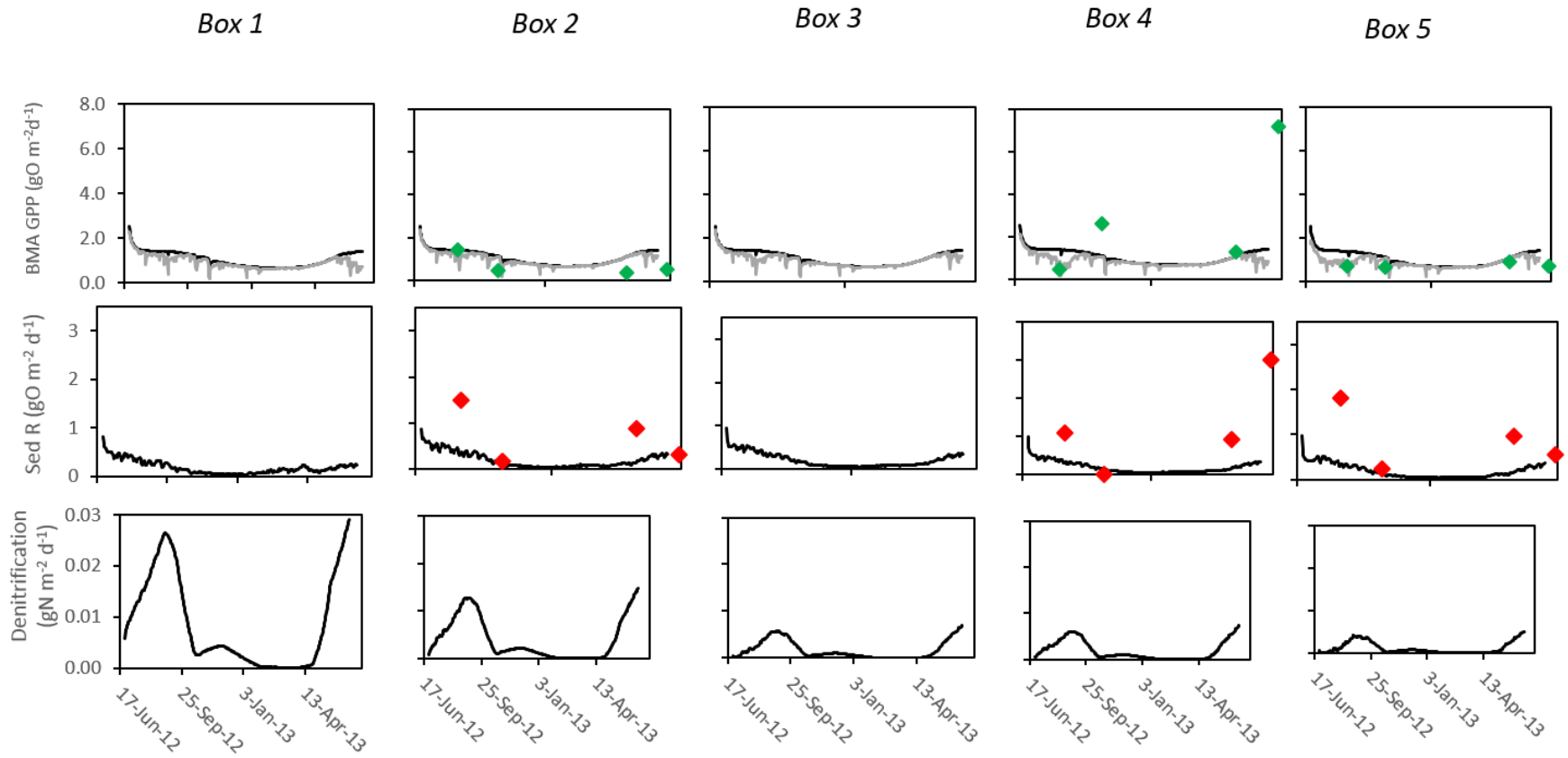
Figure 11: Measured (small diamonds) and modeled (lines) Benthic Microalgae GPP, Sediment respiration, and Denitrification. Benthic microalgae GPP was modeled in 0.0-0.5m (black lines) and 0.5-1.0 m (gray lines) depth bins, and measured GPP (diamonds) are from sediment collected at 0.5m.

54
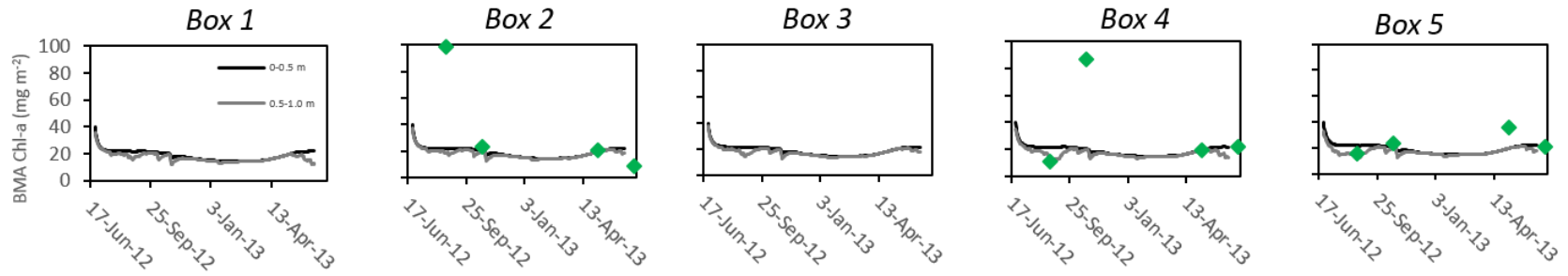
Figure 12: Measured (diamonds) and modeled (black and gray lines) Benthic Chlorophyll-a concentration in the top 3 mm Black lines depict the 0-0.5m depth bin, and gray lines depict in the 0.5- 1.0 m depth bin.
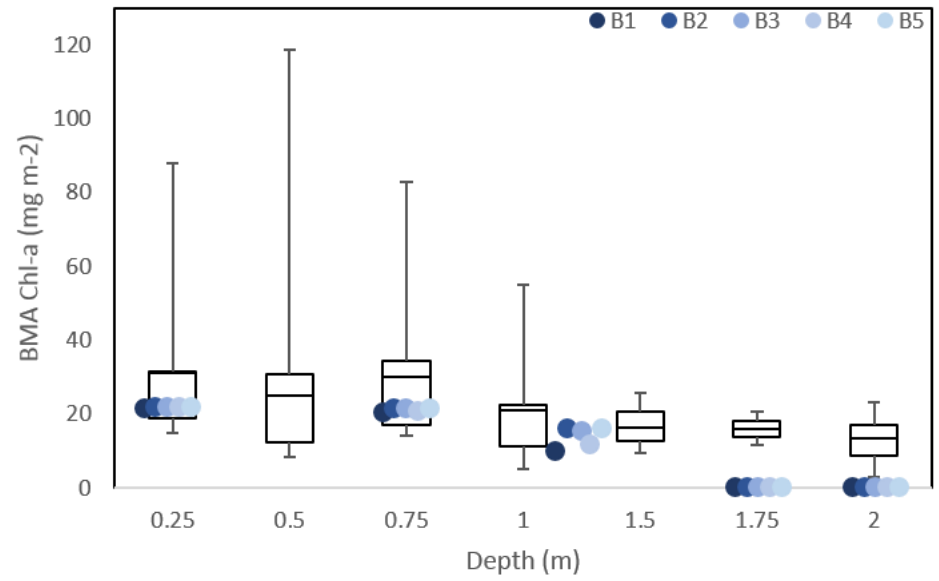
Figure 13: Benthic Microalgae Chlorophyll-*a* concentrations in the top 3 mm from the May 9, 2014 system survey (box and whiskers) and the model simulation (points) averaged for May 2013. (Points between 1 and 1.5m represent modeled values at 1.25m.)
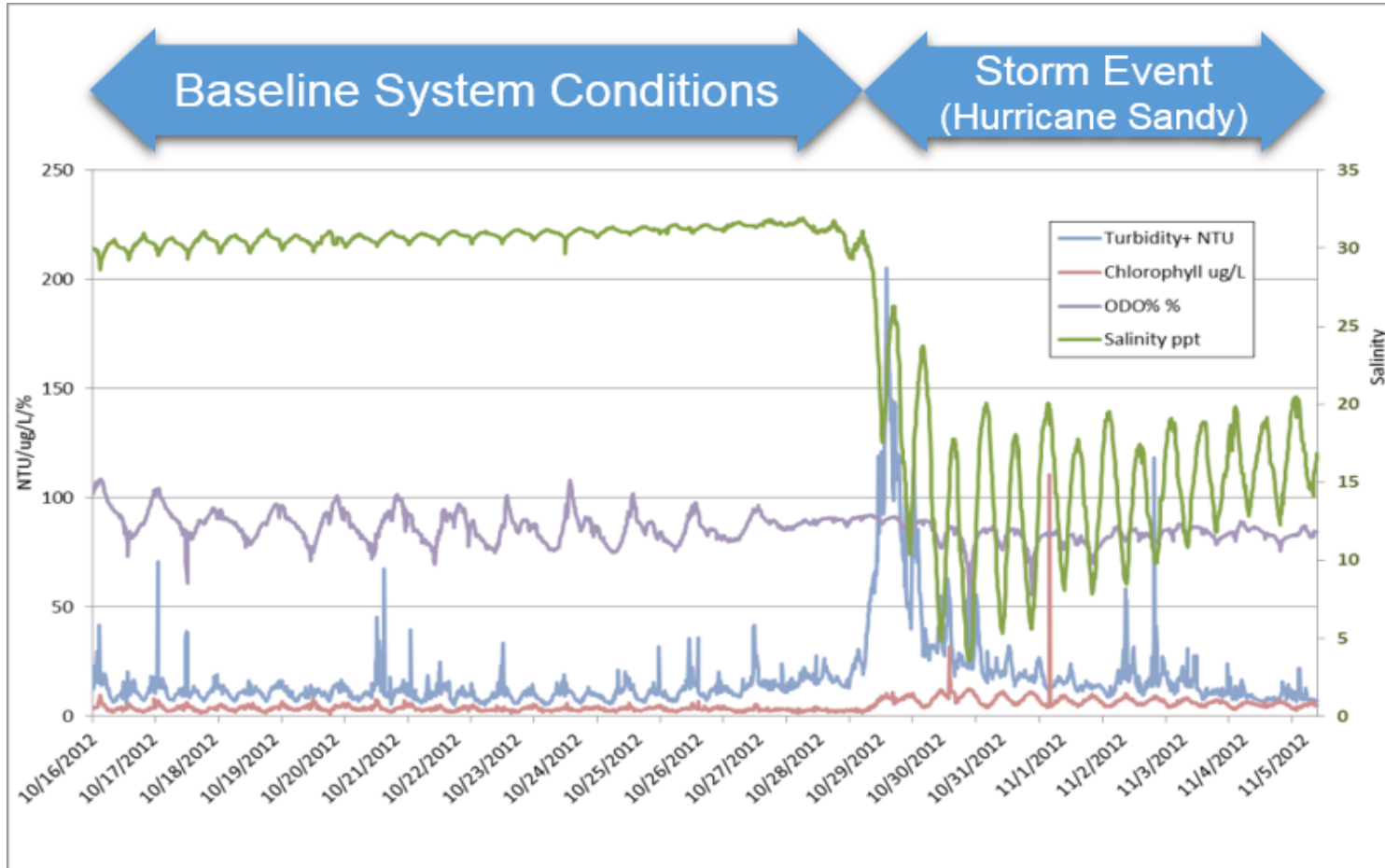
Figure 14: YSI data from the October 2012 deployment at site MH, which captured the system response to Hurricane Sandy.
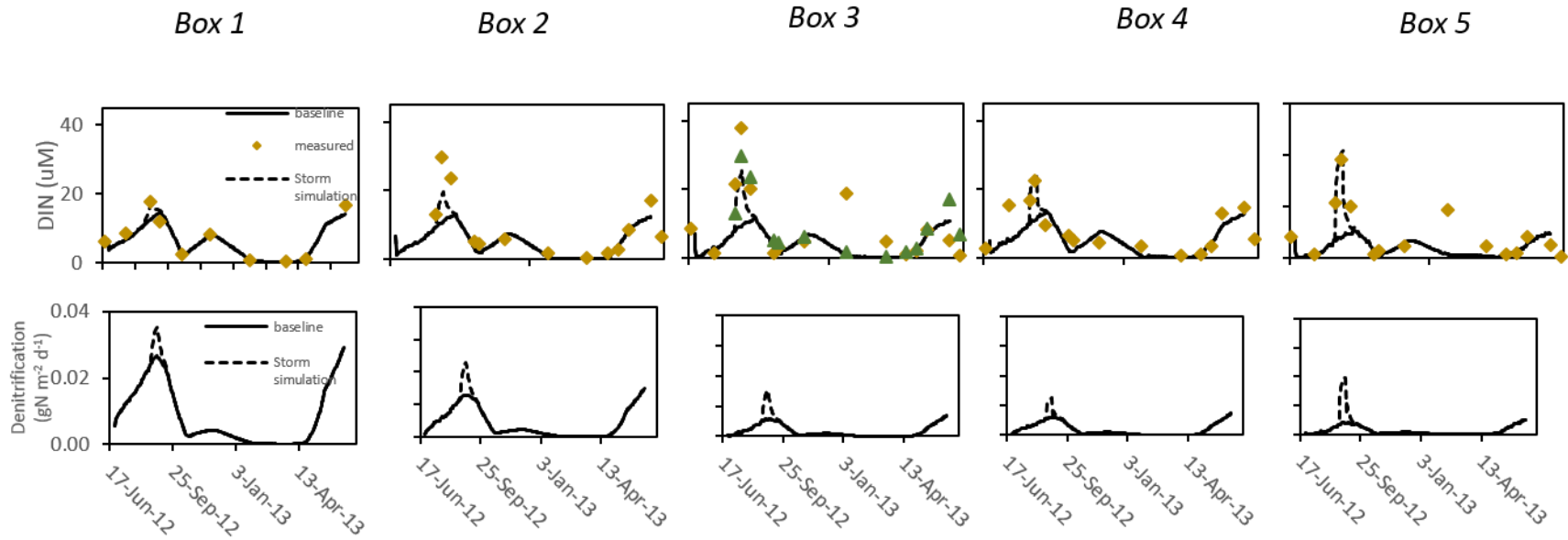
Figure 15: Model Results for DIN and denitrification from the simulation with increased nitrogen input from the August storm event. Graphs show the baseline model run (black line) with the storm simulation model run (dashed line) and measured values (diamonds and triangles) overlaid. Box 3 measured data is from the box upstream (box 5: diamonds) and downstream (box 2: triangles) as there was no data collected at this site for comparison.
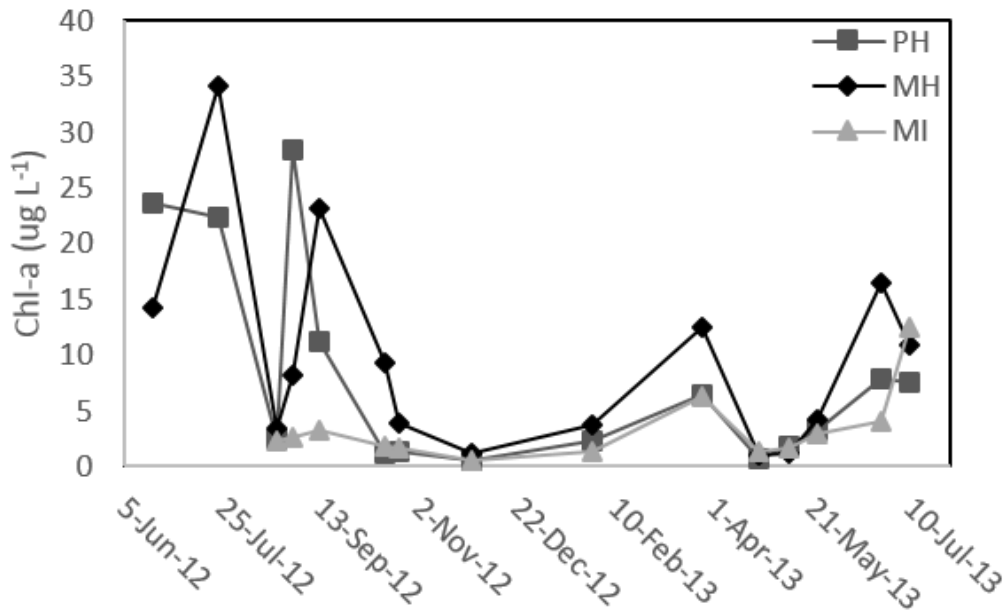
Figure 16: Water Column Chlorophyll-*a* concentration from monthly dataflow and seasonal data sets for sites PH, MH, and MI.
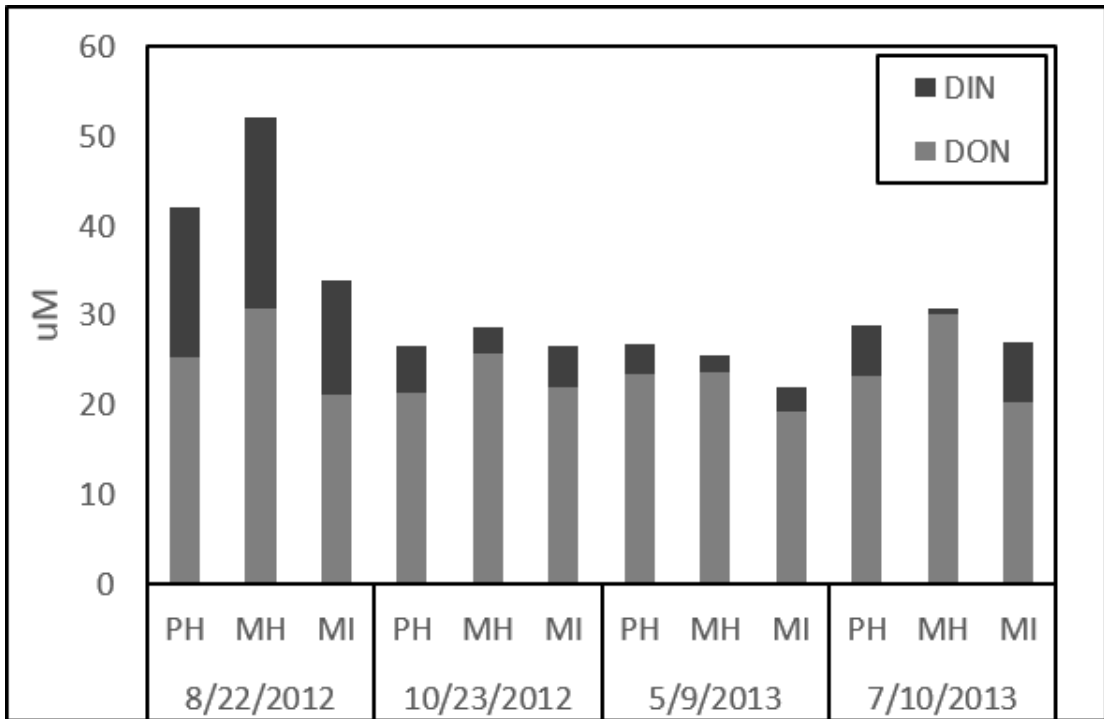
Figure 17: Water Column TDN (DIN and DON) concentrations from seasonal sampling dates at sites PH, MH, and MI.

Table 3: Annual Nutrient Budget from the baseline model run. Positive value represents net import to the GMR, and negative value represents net export from GMR.

	Box 1	Box 2	Box 3	Box 4	Box 5	All Boxes
	$(kgN\ y^{-1})$	$(kgN\ y^{-1})$	$(kgN\ y^{-1})$	$(kgN\ y^{-1})$	$(kgN\ y^{-1})$	$(kgN\ y^{-1})$
Watershed Load	7,600	2,236	6,519	9,555	17,459	43,369
Atmospheric Deposition	2,144	2,175	2,129	1,326	1,076	8,851
Exchange with HIB						
as DIN						172,830
as Phytoplankton						-61,476
Net						111,354
Phytoplankton Uptake	33,417	33,718	24,087	11,770	9,966	112,958
BMA Uptake	36,777	45,067	46,166	29,135	22,026	179,171
DNF Removal	10,706	5,078	2,083	1,433	705	20,006

Table 4: Annual Nutrient Budget from the model run with the simulated storm event. Positive value represents net import to the GMR, and negative value represents net export from GMR.

	Box 1 (kgN y⁻¹)	Box 2 (kgN y⁻¹)	Box 3 (kgN y⁻¹)	Box 4 (kgN y⁻¹)	Box 5 (kgN y⁻¹)	All Boxes (kgN y⁻¹)
Watershed Load	12,618	3,712	10,823	15,864	28,986	72,004
Atmospheric Deposition	2,144	2,175	2,129	1,326	1,076	8,851
Exchange with HIB						
as DIN						143,264
as Phytoplankton						-61,476
Net						81,788
Phytoplankton Uptake	33,417	33,718	24,087	11,770	9,966	112,958
BMA Uptake	36,777	45,067	46,166	29,088	21,986	179,083
DNF Removal	11,112	5,543	2,507	1,586	1,023	21,771

DISCUSSION

GMR System Metabolism

Component Metabolism by Season

Although Machipongo Intermediate was dominated by water column GPP and Partings Head was dominated by sediment GPP for all dates, Machipongo Head did not behave the same as either site, exhibiting a switch between water column GPP dominance in summer and sediment GPP dominance in fall and spring. The Machipongo Head site is notably not as close to the headwaters of the GMR as Partings Head is to the headwaters of Partings creek. Sediment respiration dominated over water column respiration at all sites during all dates except at Machipongo Intermediate during early summer when this site experienced the highest water column GPP of any site for any date. During the late summer Machipongo Intermediate also had the highest sediment GPP of all sites, the opposite of all other seasons in which the headwater sites had greater sediment GPP (Fig. 4). As evidenced by these data, this intermediate site is functionally different than the two headwater sites.

The headwater sites were net heterotrophic only during this late summer time period, when sediment GPP was low and sediment respiration was at the higher end of

the range for all sites over all dates (Fig. 4d-f). This suggests high amounts of

remineralization occurring in the benthos at the headwater sites during late summer.

Simultaneously in late summer, elevated water column GPP is driving net autotrophy at

MI, suggesting downstream utilization of remineralized nutrients by phytoplankton at this

site (Figs. 4 and 5). The high respiration rates in late summer are probably related to

elevated temperature as well as an observed phytoplankton bloom and subsequent crash

in late summer, which would cause a large amount of organic matter to settle on the

benthos (Fig. 16).

In comparison to a previous study of system metabolism conducted in Hog Island

Bay (Giordano et al. 2012), the timing of seasonal shifts in water column GPP and NCP

in the GMR mirrored those of HIB, with the highest rates in both systems occurring in

early and late summer. Seasonal water column GPP in HIB was 2-4x that of any

seasonal measurement in the GMR. Although water column respiration in the GMR was

in the range of rates in HIB for each season, the rates in HIB were on average 5x higher

than rates in the GMR. Opposite this trend, GMR sediment GPP was on average 0.5-3.5x

that of HIB, with HIB lying in the general range of the GMR rates (Giordano et al. 2012).

While sediment GPP was consistently higher in the GMR, sediment respiration was

generally of a similar magnitude to HIB, except for the large peak in respiration during

late summer in the GMR. Comparatively, HIB metabolism appears influenced more by

water column GPP while GMR metabolism is influenced more by sediment GPP.

Component Metabolism: Overall Averages

In addition to high overall rates of water column GPP, the Machipongo Intermediate site was characterized by benthic to pelagic GPP and respiration ratios ≤1, exhibiting a clear dominance of water column processes (Fig. 6b, e). The opposite was true of PH, which was dominated by sediment GPP and respiration with benthic to pelagic GPP and respiration ratios well over 1 (Fig 6b, e). Both headwater sites had higher average benthic respiration compared to water column respiration, but MH had a more balanced ratio of water column to sediment GPP (Fig 6a, d).

Overall, HIB water column metabolism was 3x that in the GMR, while sediment metabolism in the GMR was 2-3x that of HIB (Giordano et al. 2012). All sites in the GMR and HIB studies were on average net autotrophic, with the GMR exhibiting half the magnitude of HIB NEM (Fig 6c, f). HIB was characterized as having benthic to pelagic GPP ratios well below 1, and experienced autotrophic NEM driven by phytoplankton production. Benthic drivers led to higher GPP in the headwaters of the GMR, suggesting autotrophy is driven by benthic production throughout much of the GMR.

Average net autotrophy in the GMR suggests utilization and transformation of watershed nutrients by both phytoplankton and benthic microalgae. The seasonal pattern of heterotrophy at sites MH and PH during the late summer suggest that high respiration rates are remineralizing biomass into dissolved nitrogen, consistent with late summer temperature increases.

Open Water Metabolism and Comparison to Component Rates

At sites PH and MH, open water and component sites were directly adjacent and thus directly comparable (Fig 1). Conversely, while sites MM and MI are used for comparisons, site MM was located downstream from site MI (Fig 1). MI and MM sites are similar in that they are both further down estuary and deeper than the headwater sites.

A large peak in heterotrophy based on the open water method at PH and MH in late summer is in agreement with net heterotrophy measured from the component method (Fig 7). Beyond that season, no patterns between open water and component NEM were apparent, with open water and component methods disagreeing on metabolic status (Fig 8). Often the results of the open water method show system heterotrophy, and rarely are the two approaches used simultaneously to assess the same system (Caffrey 2004; Gazeau 2005; Testa et al. 2013). In the Giordano et al. (2012) assessment of NEM in Hog Island Bay, the two methods were applied simultaneously, and similar to our study, the results did not agree on system heterotrophy or autotrophy. Although the two methods disagree, multiple spatial and temporal assessments of open water metabolism combined with container incubations, such as those in this study, can give clues as to system function and varied autotroph dominance.

The disagreement in these two methods is possibly due to a few key factors. The component method works best when metabolism in all habitats is assessed, but this is not always logistically feasible or entirely informative. Our component analysis did not include two main habitats of the system: large intertidal marshes and temporal macroalgae blooms. Metabolic functioning of the marsh system was beyond the scope of this project, and in the beginning of this study it was unknown whether or not macroalgae blooms were occurring in the GMR. A macroalgae bloom was observed throughout

many parts of the system during the benthic chlorophyll survey conducted in mid-May of 2014. A bloom was not seen during the year of major sampling (2012-2013), although this does not mean one did not occur as macroalgae blooms are ephemeral in nature. Macroalgal GPP and respiration were measured in the aforementioned component analysis of Hog Island Bay, and the addition of macroalgal metabolism caused sediment metabolism to shift to heterotrophy during the peak bloom season May-July, but did not affect the overall trophic state of the system (Giordano et al. 2012). Due to its patchy nature, difficulty in scaling up to the whole system, and limited contribution to metabolism in the Giordano et al. (2012) study, macroalgae were excluded from this study.

Additionally, a major assumption of the open water method is that the same water mass is being sampled over the course of a day (Caffrey 2004). With average depths of 0.5 - 1.25 m and a tidal range of 1.25 m in the GMR, water masses move considerably throughout the day and night. Most notably, in this system the water mass is filling and draining the expansive intertidal marshes twice daily due to tidal flooding. Marshes have been shown to deliver low oxygen water high in dissolved inorganic carbon to surrounding waters, which can contribute to an apparent heterotrophic signal when using the open water NEM method (Neubauer and Anderson 2003, Raymond et al. 2000). Because this delivery of low oxygen water is not a signal of bacterial consumption of organic matter in the water column, which was the focus of this study, apparent open water heterotrophy may not be an accurate characterization of GMR function. Giordano et al. (2012) attempted to correct for this discrepancy by including marsh respiration rates in open water metabolism calculations in HIB with mixed results.

A comparative analysis across systems shows that the ratio of DIN to organic

carbon inputs can predict whether a system will be net heterotrophic or autotrophic (Testa

et al. 2013; Hopkinson and Vallino, 1995; Kemp et al. 1997; Gazeau et al. 2005). Based

on the loads used in the model, this ratio in the GMR is 1.43 mol mol $^{-1}$, which places the

system well into the autotrophic area of the curve in the aforementioned study and

confirms our reliance on the component method results. In this study we believe the

component method results in a better representation of material processing directly within

the GMR creek and sediments due to directly measured metabolic rates and the

limitations of the open water method in this system. Additionally, the component method

allowed for direct characterization and comparison of the water column and sediments.

GMR Ecosystem Model

State Variables and Metabolic Rates

All state variable predictions from the model are within the magnitude of the

measured values, and the majority of seasonal trends in these stocks are being captured,

providing confidence in model outcomes. It is expected that the model should

underpredict the magnitude of large water column and benthic chlorophyll-a blooms,

seen in the water column during late summer and the benthos during early summer (Figs.

9 and 11), due to their short-lived nature, limited sampling frequency of the study, and

coarse resolution of model boxes and inputs. While the model may not capture the

magnitudes of these peaks and valleys, the simulation is providing a robust snapshot of overall system function through the simulation year.

The underprediction of sediment respiration and water column chlorophyll-*a* in the upper estuary boxes during late summer are most likely driving the simultaneous overprediction of the O_2 pool (Figs. 9 and 10). From the component metabolism studies we know sediment respiration is driving net heterotrophy in boxes 4 and 5 in late summer. We believe the model is not capturing the magnitude of nutrient remineralization occurring in the sediments in late summer. Enhanced remineralization would add to the pool of modeled DIN, where it is currently being underpredicted, which would increase water column chl-a, and draw down the high modeled water column DO concentrations. The increased nutrient availability in the water column could then lead to an increase in water column chlorophyll-a

Although measured rates of denitrification for the GMR are unavailable, the modeled rates of denitrification in boxes 2-5 fell within the range of measured rates in Hog Island Bay and surrounding tributary creeks of 0-0.02 and 0.0006-0.01 g m^{-2} d^{-1}, respectively (Anderson, unpublished data; Fig 11). Box 1 had the highest rate of denitrification and has the greatest average depth of all boxes at 2.2 m, with some places 12-18 m deep. This higher rate of denitrification experienced in Box 1 is not unexpected as Hog Island Bay only has an average depth of 1-2 m. Compared to boxes 2-5, a deeper benthos in box 1 means a smaller photic benthic area and thus less active BMA, which would lead to less oxygenated sediments, less competition for nitrate, and a greater potential for increased denitrification.

Average rates of denitrification for all boxes ranged from 0.079 to 0.606 mmol N m^{-2} d^{-1}, falling within the range of rates (0-38 mmol N m^{-2} d^{-1}) compiled by Joye and Anderson (2008). Although the GMR rates are at the lower end of this range, more in line with values from continental shelf habitats than higher values from shallow coastal systems, lower rates in the GMR are not surprising due to the presence of benthic microalgae and a large tidal range to depth ratio, which serve to oxygenate the sediments and inhibit denitrification. The large tidal range in the GMR also leads to a very low flushing time, which has been associated with a lower fraction of nitrogen inputs being lost to denitrification (Nixon et al. 1996).

The depth survey of benthic chlorophyll-a concentrations indicates that the model is underestimating BMA concentrations, particularly at deeper depths (Fig. 13). This apparent underestimation could be an artifact of the light attenuation coefficient calculation in the model, but is most likely due to the fact that the modeled data set and benthic chlorophyll-a survey were conducted during the same season, but different years. Although the measurements are not directly comparable, it is encouraging that most of the modeled concentrations lie within the range of the observations, and the model reproduces the observed decline with depth. Seasonally, the model is capturing an increase, but underprecting the magnitude of BMA chlorophyll-a concentrations in box 2 during late summer, box 4 during fall, and box 5 during the spring bloom. These lines of evidence lead us to believe that if anything, the prediction of benthic primary productivity and nutrient processing in this study is conservative.

Total modeled primary productivity of pelagic and benthic autotrophs in the GMR was 116 g C m^{-2} y^{-1}. In comparison to primary productivity in other systems, the GMR

lies in the most frequent category of pelagic dominated systems, 100-199 g C m^{-2} y^{-1}, but well below the most frequent rates seen in systems that include benthic producers, 301-400 g C m^{-2} y^{-1} (Boynton and Kemp 2005). This could be due to the exclusion of macroalgal and salt marsh production in this study or possibly the very shallow water column, high levels of turbidity, and rapid flushing rates. Additionally, under-predicted phytoplankton standing stock in the late summer months and exclusion of the high early summer GPP rates in the model could be contributing to this likely underestimate.

System Nutrient Budget

Baseline Model Simulation

Exchange across the mouth of the GMR indicates the creek is importing over three times the amount of N coming from the atmosphere and watershed combined, in the form of DIN from HIB (Table 3). The net import of N from HIB decreases by a third when accounting for the N in phytoplankton being exported to HIB (Table 3). The net import of N from HIB indicates that the GMR is a sink for N, and the net import of DIN and export of particulate organic phytoplankton N indicates the system is acting as a substantial nutrient transformer. Total inputs of N from the atmosphere and watershed combined are approximately equal to the N present in exported phytoplankton biomass, suggesting the system is effectively transforming watershed- and atmosphere-derived DIN into phytoplankton biomass.

It is probable that the form of nitrogen being exchanged with HIB is not only as DIN and phytoplankton biomass, but also DON. Currently there is not a pool for DON in the model, so the GMR is possibly exporting large amounts of DON to HIB while importing DIN. In the aforementioned metabolism study of HIB, DON comprised approximately 83% of total dissolved nitrogen (TDN) in the bay, suggesting this may be the case (Giordano et al. 2012; McGlathery et al. 2007). In addition, a five year study conducted in HIB found DON was a similarly large portion of the TDN pool at >75% (Anderson et al. 2010). Conversely, a study of baseflow N loading in the creeks of the Virginian Eastern Shore found DIN was the greatest percentage of TDN, ranging from 66% to 98% (Stanhope et al. 2009). During the seasonal sampling in this study, 2% - 41% of TDN was DIN, with an average of 20.3% (Fig. 17). While this percentage varies considerably in the GMR depending on season and condition, percent DIN in the GMR is on average lower than values in watershed inputs and higher than those in the adjacent bay.

Possible sinks for N that are not accounted for in our model are uptake by the intertidal marshes, ephemeral macroalgal blooms, and burial. Additionally, the formulation of BMA in this model includes their ability to draw nutrients from the water column or benthos, representative of actual behavior. This can introduce a source of nitrogen to the modeled system not otherwise accounted for in N inputs from the watershed. This inexhaustible pool of DIN in the benthos means the budget presented in this study is not a closed budget, but nonetheless it is a useful way to examine relative amounts of major inputs and internal processes. Anderson et al. (2010) estimated that in addition to the watershed load of N, 33% more N enters HIB from direct groundwater

discharge. This extra pool of N in the model serves to add to the amount of nitrogen taken up by the BMA, known to act as a temporary filter in shallow estuarine systems.

The modeled internal rates of phytoplankton and benthic microalgal uptake of N are 216 and 343% of watershed plus atmospheric N inputs, respectively. The GMR is thus a major transformer of DIN inputs, and while phytoplankton represent only a transformation, benthic microalgae have been shown to act as a temporary sink or filter by capping the flux of N out of the sediments to the overlying water column (Anderson et al. 2003; McGlathery et al. 2007; Joye and Anderson 2008). Total denitrification in the system is 38% of watershed plus atmospheric inputs, a relatively small amount in comparison to the nutrient transformations occurring in the autotrophic community. This denitrification, although expectedly low due to the rapid flushing of the system (Nixon et al. 1996), represents a permanent sink. The GMR system is efficiently utilizing N inputs by acting as a permanent sink for almost half of the land based inputs and as a transformer and temporary sink for the remainder.

Benthic microalgal N uptake is an important component of N processing throughout the entire GMR with total BMA uptake per box much larger than that of total phytoplankton uptake. BMA and phytoplankton uptake rates are similar in box 1, near HIB, and diverge upstream towards the headwater boxes 3 and 5, where BMA uptake is twice that of phytoplankton uptake. However, the model is under-predicting water column chlorophyll-a in boxes 4 and 5, so the actual difference may not be this pronounced. This modeled gradient in BMA and phytoplankton uptake reflects the pattern of benthic: pelagic GPP observed in metabolic incubations.

Anderson et al. (2003) found benthic microalgae to be extremely important in capping nutrient fluxes from the benthos to the water column. Modeled rates of BMA uptake in this study were consistently greater than rates of nutrient mineralization. This resulted in a negligible or negative net flux of N to the water column from the sediments. These results suggest that BMA and the sediment microbial community are tightly coupled and provide a cap on any nutrients coming out of the sediment (Anderson et al. 2003; Anderson et al. 2010). In these earlier analyses the authors state that the calculated BMA rates are probably overestimated due to use of GPP measured only in the light. In this study, we found that our modeled uptake of N by BMA was indeed lower than that in HIB. The modeled BMA uptake, or nitrogen demand, for the growing season was 2.1-4.2 mmol N m^{-2} d^{-1}, compared to 7.4-10.8 mmol N m^{-2} d^{-1} calculated at the creek site of the HIB study (Anderson et al. 2003). The BMA uptake rates in our study are very close to the mineralization rates measured in the HIB study, suggesting that even with these lower rates of N demand, the GMR could be capable of a negligible or negative net flux of N from the sediments.

Storm Model Simulation

The late summer storm simulation served only to increase the DIN pool and denitrification rates slightly within the model (Fig. 15). No other state variables were affected and almost all of the excess DIN was flushed from system (Table 4). Because this system has such a small watershed to open water ratio, with very little freshwater inflow and a high flushing rate, large storm events lead to nutrient pulses and scouring

with subsequent organic matter export. The stochastic nature of this system suggests that these tidal creeks function differently during baseflow and storm conditions. In simulating the storm event, we did not increase the volume of tidal exchange within the system, which would possibly serve to increase flushing of materials. This storm simulation confirms the system acts as a conduit for nutrients to the outer bays during large storm events, and because we only simulated one storm event and did not increase tidal flushing, the conduit role of the creeks is most likely a conservative estimate.

CONCLUSIONS

Net autotrophic ecosystem metabolism, calculated using the component method, is in agreement with the model results, that the GMR functions as a major transformer and filter of watershed nutrients. Conversely, the system appears to function more as a conduit for watershed nutrients during large storm events. The model and metabolic results also agree in the increasingly important role of benthic autotrophs moving up the GMR from HIB to the headwater sites. This is evidenced by the benthic to pelagic GPP ratios in the metabolism study and rates of BMA and phytoplankton uptake rates from the model. Consequently, denitrification has a more important role in N processing moving downstream from the headwater sites to HIB. BMA is only considered a temporary filter, but its continued presence in a system can act to cap any N coming from groundwater discharge. Higher denitrification rates of the downstream sites suggest they are removing more N from the system than those of the headwaters. Both of these outcomes highlight the major role played by the benthos in the functioning of the GMR ecosystem.

Future studies of marsh plant and marsh sediment metabolic rates could go a long way to fill gaps of this study. These rates could be incorporated into component studies to potentially resolve the discrepancy with the open water results, and inclusion of these rates in the model formulation would shed even more light on the relative importance of each habitat to the overall functioning of the GMR. If primary productivity of the extensive marsh system as well as macroalgal blooms were to be included, the overall

productivity of the system could possibly increase to be in the expected range for shallow

coastal systems.

LITERATURE CITED

Accomack County. Respecting the past, creating the future: Accomack county comprehensive plan. May 14, 2008.

Accomack County. *Draft* Chapter 6: Future Land Use Plan from "Respecting the past, creating the future: Accomack county comprehensive plan". February 4, 2014.

Alpine, AE, and JE Cloern. 1992. Trophic interactions and direct physical effects control phytoplankton biomass and production in an estuary. Limnology and Oceanography, *37*(5), 946-955.

Anderson, IC, McGlathery, KJ, and AC Tyler. 2003. Microbial mediation of 'reactive' nitrogen transformations in a temperate lagoon. Marine Ecology Progress Series, 246, 73-84.

Anderson, IC, Stanhope, JW, Hardison, AK, and KJ McGlathery. 2010. Sources and fates of nitrogen in Virginia coastal bays. pp 43-72 in: Kennish, MJ and HW Pearl (eds), Coastal lagoons: critical habitats of environmental change. CRC Press, Boca Raton, FL.

Borum, J and K Sand-Jensen. 1996. Is total primary production in shallow coastal marine

waters stimulated by nitrogen loading? Oikos 76 (2): 406-410.

Boynton WR, Hagy JD, Cornwell JC, Kemp WM, Greene SM, Owens MS, Baker JE, and Larsen RK. 2008. Nutrient budgets and management actions in the Patuxent River Estuary, Maryland. Estuaries and Coasts 31:623-651.

Boynton, WR, Hagy, JD, Murray, L, Stokes, C, and WM Kemp. 1996. A comparative analysis of eutrophication patterns in a temperate coastal lagoon. Estuaries 19 (2B): 408-421.

Boynton, W.R., and Kemp, W.M., 2005. Nitrogen in Estuaries. In: Capone, D.G., Bronk, D.A., Mullholland, M.R., Carpenter, E.J., 2006. Nitrogen in the Marine Environment.

Brush, MJ. 2010. Forecasting the response of Delmarva lagoons to changing land use and climate: alternative stable states and recovery trajectories. Regional DE-MD-VA Sea Grant demo project Fall 2010 Progress Report.

Brush, MJ, JW Brawley, SW Nixon, and JN Kremer. 2002. Modeling phytoplankton production: problems with the Eppley curve and an empirical alternative. Marine Ecology Progress Series 238:31-45.

Brush, MJ and LA Harris. 2010. Introduction to the special issue of *Ecological Modelling:* "Advances in modeling estuarine and coastal ecosystems: approaches, validation, and applications". Ecological Modelling 221: 965-968.

Brush, MJ and LA Harris. 2016. Ecological Modeling. Pp. 214-223 in: Kennish, M.J.(ed.), Encyclopedia of Estuaries, Encyclopedia of Earth Sciences Series, Springer Netherlands.

Brush MJ, Harris LA, York JK, Kroeger KD, Anderson IC, and Boynton WR. 2012. Sea Grant Proposal: Forecasting watershed loading and lagoon response along the Delmarva Peninsula due to changing land use and climate.

Brush, MJ and Nixon, SW. 2010. Modeling the role of macroalgae in a shallow sub-estuary of Narragansett Bay, RI (USA). Ecological Modelling 22: 1065-1079.

Buzelli, C. 2008. Development and application of tidal creek ecosystem models. Ecological Modelling 210: 127-143.

Caffrey, J.M. 2003. Production, Respiration and Net Ecosystem Metabolism in U.S. Estuaries. Environmental Monitoring and Assessment. 81: 207-219.

Cerco, CF and T Cole. 1993. Three-dimensional eutrophication model of Chesapeake Bay. Journal of Environmental Engineering 119(6): 1006-1025.

Cloern, JE. 2001. Our evolving conceptual model of the coastal eutrophication problem. Marine Ecology Progress Series 210: 223-253.

Cole, L.W. 2005. Nitrogen loading to Chincoteague Bay (MD, VA): a reassessment. MS thesis, University of Rhode Island, Kingston, RI. 91 pp.

Duarte, C. M., J. S. Amthor, D. L. DeAngelis, L. A. Joyce, R. J. Maranger, M. L. Pace, J. Pastor, and S. W. Running. 2003. The limits to models in ecology. Pages 437-451 in C. D. Canham, J. J. Cole, and W. K. Lauenroth, editors. Models in ecosystem science. Princeton University Press, Princeton, New Jersey, USA.

Fugate, DC, Friedrichs, CT, and A Bilgili. 2005. Estimation of residence time in a shallow back barrier lagoon, Hog Island Bay, Virginia, USA. In International Conference on Estuarine and Coastal Modeling, Charleston, South Carolina, USA.

Giordano, JCP. 2009. Nutrient loading and system response in the coastal lagoons of the Delmarva Peninsula. M.S. thesis, College of William and Mary, Virginia Institute of Marine Science, Gloucester Point, Va.

Giordano, JCP, Brush, MJ, and IC Anderson. 2011. Quantifying annual nitrogen loads to Virginia's coastal lagoons: sources and water quality response. Estuaries and Coasts 34: 297-309.

Giordano, JCP, Brush, MJ, and IC Anderson. 2012. Ecosystem metabolism in shallow coastal lagoons: patterns and partitioning of planktonic, benthic, and integrated community rates. Marine Ecology Progress Series 458: 21-38.

Hardison, AK, Anderson, IC, Canuel, EA, Tobias, CR, and B Veuger. 2011. Carbon and nitrogen dynamics in shallow photic systems: interactions between macroalgae, microalgae, and bacteria. Limnology and Oceanography 56(4): 1489-1503.

Hardison, AK, Canuel, EA, Anderson, IC, and B Veuger. 2010. Fate of macroalgae in benthic systems: carbon and nitrogen cycling within the microbial community. Marine Ecology Progress Series 414: 41-55.

Herman, J, Shen, J, and J. Huang. 2007. Tidal Flushing Characteristics in Virginia's Tidal Embayments, Final Report to Virginia Coastal Zone Management Program and Virginia Department of Environmental Quality by Center for Coastal Resources Management Grant #NA06N0S4190241.

Hopkinson CS, Smith EM (2005) Chapter 8: Estuarine respiration: An overview of benthic, pelagic and whole system respiration. In P.A. del Giorgio and P.J. le B. Williams (Eds.), Respiration in aquatic ecosystems. Oxford University Press. pp 123-147

Hopkinson, CS and JJ Vallino. 1995. The relationships among man's activities in watersheds and estuaries: A model of runoff effects on patterns of estuarine community metabolism. Estuaries 18(4): 598-621.

Howarth, RW and R Marino. 2006. Nitrogen as the limiting nutrient for eutrophication in coastal marine ecosystems: evolving views over three decades. Limnology and Oceanography 51 (1.2): 364-376

Howarth, RW. 1998. An assessment of human influences on fluxes of nitrogen from the terrestrial landscape to the estuaries and continental shelves of the North Atlantic Ocean. Nitrogen Cycling in Agroecosystems 52(2): 213-223.

Jassby, AD and T Platt. Mathematical formulation of the relationship between photosynthesis and light for phytoplankton. Limnology and Oceanography 21(4): 540-547.

Joye, SB and IC Anderson. 2008. Nitrogen cycling in Estuarine and Nearshore Sediments. In: Capone, D., Bronk, D., Carpenter, E. and Mulhollond, M. (Eds), Nitrogen in the Marine Environment, Springer Verlag, Chapter 19, pp 868-915.

Kemp, WM and WR Boynton. 1980. Influence of biological and physical processes on dissolved oxygen dynamics in an estuarine system: implications for measurement of community metabolism. Estuarine and Coastal Marine Science. II: 407-431.

Kemp, WM, Smith, EM, Marvin-DiPasquale, M, and WR Boynton. 1997. Organic carbon balance and net ecosystem metabolism in Chesapeake Bay. Marine Ecological Progress Series 150: 229-248.

Kemp, WM, and Boynton, WR. 2012. Synthesis in estuarine and coastal ecological research: what is it, why is it important, and how do we teach it. Estuaries and Coasts 35:1-22.

Kemp, W M, and JM Testa (2011). Metabolic balance between ecosystem production and consumption. Treatise on estuarine and coastal science, 7.

Knepel K, Bogren, K. 2001. Determination of orthophosphate by flow injection analysis. QuikChem Method 21-115-01-1-H. Lachat Instruments, Milwaukee, WI.

Kremer JN, Nixon SW (1978) A coastal marine ecosystem: simulation and analysis. Springer-Verlag, New York

Kremer, JN, Reischauer, A and C D'Avanzo. 2002. Estuary-specific variation in the air-water gas exchange coefficient for oxygen. Estuaries 26(4):829-836.

Lake, SJ and MJ Brush. 2011. The contribution of microphytobenthos to total productivity in Narragansett Bay, Rhode Island. Estuarine, Coastal, and Shelf Science 95:289-297.

Lake, SJ, Brush, MJ, Anderson, IC and HI Kator. 2013. Internal versus external drivers of periodic hypoxia in a coastal plain tributary estuary: the York River, Virginia. Marine Ecology Progress Series 492: 21-39.

Lake, SJ and MJ Brush. 2015. Contribution of Nutrient and Organic Matter Sources to the Development of Periodic Hypoxia in a Tributary Estuary. Estuaries and Coasts 38(6): 2149-2171.

Liao, N. 2001. Determination of ammonia in brackish or seawater by flow injection analysis. QuikChem Method 21-107-06-1-B. Lachat Instruments, Milwaukee, WI.

Lorenzen, C. 1967. Determination of chlorophyll and phaeopigments: spectrophotometric equations. Limnology and Oceanography 12:343-346.

Lucas, LV, Thompson, JK, and LR Brown. 2009. Why are diverse relationships observed between phytoplankton biomass and transport time. Limnology and Oceanography, 54(1), 381-390.

Marino, R and RW Howarth. 1993. Atmospheric oxygen exchange in the Hudson River: dome measurements and comparison with other natural waters. Estuaries 16: 433-445.

Ménesguen, A., P. Cugier, S. Loyer, A. Vanhoutte-Brunier, T. Hoch, J. F. Guillaud, and F. Gohin. 2007. Two- or three-layered box-models versus fine 3D models for coastal ecological modelling? A comparative study in the English Channel (Western Europe). Journal of Marine Systems 64:47-65.

Mcglathery, KJ, Anderson, IC, and AC Tyler. 2001. Magnitude and variability of benthic and pelagic metabolism in a temperate coastal lagoon. Marine Ecology Progress Series 216: 1-15.

McGlathery, KJ, Sundback, K, and IC Anderson. 2007. Eutrophication in shallow coastal bays and lagoons: the role of plants in the coastal filter. Marine Ecology Progress Series 348:1-18.

Monsen, NE, Cloern, JE, Lucas, LV, and SG Monismith. 2002. A comment on the use of flushing time, residence time, and age as transport time scales. Limnology and Oceanography, 47(5), 1545-1553.

Nixon, SW. 1995. Coastal marine eutrophication: a definition, social causes, and future concerns. Ophelia 41:199-219.

Nixon, SW, Ammerman, JW, Atkinson, LP, Berounsky, VM, Billen, G, Boicourt, WC, & SP Seitzinger. 1996. The fate of nitrogen and phosphorus at the land-sea margin of the North Atlantic Ocean. In Nitrogen cycling in the North Atlantic Ocean and its Watersheds (pp. 141-180). Springer Netherlands.

Nixon, S, Buckley, B, Granger, S, and J Bintz. 2001. Response of very shallow marine ecosystems to nutrient enrichment. Human and Ecological Risk Assessment 7:1457-1481.

Nixon, SW, Fulweiler, RW, Buckley, BA, Granger, SL, Nowicki, BL, and KM Henry. 2009. The impact of changing climate on phenology, productivity and benthic-pelagic coupling in Narragansett Bay. Estuarine, Coastal and Shelf Science 82: 1-18.

Northampton County. Northampton county comprehensive plan update. April 14, 2009.

Northampton County Comprehensive Plan Advisory Committee. "Bridges of Hope: Strenthening the Economy of Northampton County" Presentation to Northampton County Board of Supervisors. February 12, 2013.

NRC (National Research Council). 2000. Clean coastal waters: understanding and reducing the effects of nutrient pollution. National Academy Press, Washington, DC.

Officer, CB. 1980. Box Models Revisited. Pp.65-114 *in*: Hamilton, P and KB MacDonald (eds.). Estuarine and wetland processes with emphasis on modeling. Plenum Press, New York.

Pemberton, M, Anderson, GL, and JH Barker. 1996. Characterization of microvascular vasoconstriction following ischemia/reperfusion in skeletal muscle using videomicroscopy. Microsurgery 17:9-16.

Pinckney J, Zingmark RG. 1993. Biomass and production of benthic microalgal communities in estuarine habitats. Estuaries 16:887-897.

Platt, T, Gallegos, CL, Harrison, WG. 1980. Photoinhibition of photosynthesis in natural assemblages of marine phytoplankton. J Mar Res 38:687-701.

Pritchard, DW. 1960. Salt balance and exchange rate for Chincoteague Bay. Chesapeake Science 1, 48-57.

Rabalais, NN, Turner, RE, and WJ Wiseman Jr. 2002. Gulf of Mexico Hypoxia, aka "The Dead Zone". Annual Review of Ecology and Systematics 33: 235-263.

Robinson, MA, and WG Reay. 2002. Ground water flow analysis of a Mid-Atlantic outer coastal plain watershed, Virginia, USA. Ground Water 40(2):123-131.

Shoaf, WT, Lium, BW. 1976. Improved extraction of chlorophyll a and b from algae using dimethyl sulfoxide. Limnology and Oceanography 21:926-928.

Smith, P, Bogren, K. 2001. Determination of nitrate and/or nitrite in brackish or seawater by flow injection analysis colorimetry. QuikChem Method 31-107-04-1-E. Lachat Instruments, Milwaukee, WI.

Shen, J, and HV Wang. 2007. Determining the age of water and long-term transport timescale of the Chesapeake Bay. Estuarine, Coastal and Shelf Science, 74(4), 585-598.

Sheremet, VA, 2010. Observations of Near-Bottom Currents with Low-Cost SeaHorse Tilt Current Meters. Report for grant N00014-09-1-0993, Office of Naval Research, 7 pp.

Staehr, PA, Testa, JM, Kemp, WM, Cole, JJ, Sand-Jensen, K, and SV Smith. 2012. The metabolism of aquatic ecosystems: history, applications, and future challenges. Aquatic Science 74:15-29.

Stanhope, JW, Anderson, IC, and WG Reay. 2009. Base flow nutrient discharges from lower Delmarva Peninsula watersheds of Virginia, USA. Journal of Environmental Quality 38(5):2070-2083.

Testa, JM, Kemp, WM, Boynton, WR, and JD Hagy III. 2008. Long-term changes in water quality and productivity in the Patuxent River Estuary: 1985 to 2003. Estuaries and Coasts 31: 1021-1037.

Testa, JM and WM Kemp. 2008. Regional, seasonal, and inter-annual variability of biogeochemical processes and physical transport in a partially stratified estuary: a box-modeling analysis. Marine Ecology Progress Series 356:63-79.

Testa, JM, Kemp, WM, Hopkinson, CS, and SV Smith. 2012. Ecosystem Metabolism pp 381-416 in: Estuarine Ecology. John Wiley & Sons, Ltd.

Testa, JM, Brady, DC, Di Toro, DM, Boynton, WR and WM Kemp. 2013. Sediment flux modeling: Nitrogen, phosphorous and silica cycles. Estuarine Coastal and Shelf Science 117:245-263.

U.S. Environmental Protection Agency, 1971. Method 160.4: Residue, Volatile (Gravimetric, Ignition at 550°C)

U.S. Environmental Protection Agency, 1971. Method 160.2: Residue, Non-Filterable (Gravimetric, Dried at 103-105°C)

Valiela, I. 1995. Marine Ecological Processes (2nd Edition). Springer; Chapter 13 – The carbon cycle: production and transformations of organic matter

Valiela, I, McClelland, J, Hauxwell, J, Behr, PJ, Hersh, D and K Foreman. 1997.

Macroalgal blooms in shallow estuaries: controls and ecophysiological and ecosystem

consequences. Limnology and Oceanography 42(5.2):1105-1118.

Wanninkhof, R. 1992. Relationship between wind speed and gas exchange over the

ocean. Journal of Geophysical Research 97(C5): 7373-7382.

Wang, T. 2009. Numerical modeling of eutrophication dynamics in the shallow coastal

ecosystem: a case study in the Maryland and Virginia bays (Doctoral dissertation).

College of William and Mary.

Zimmerman, JTF. 1988. Estuarine residence times, p. 75-84. *In* B. Kjerve [ed.],

Hydrodynamics of estuaries. V. 1. CRC Press.